

# Emerging nanostructured infrared absorbers enabling cost-effective image sensing: a review

Neena Gupta,<sup>a</sup> Jyoti Kedia,<sup>a</sup> and Anurag Sharma<sup>a,b,\*</sup>

<sup>a</sup>Punjab Engineering College (Deemed to be University), Department of Electronics and

Communication Engineering, Chandigarh, Punjab, India

<sup>b</sup>Chandigarh University, Gharuan, Punjab, India

**Abstract.** Image sensing has entered a new era with advancements in quantum mechanics. The infrared (IR) absorbers are the heart of this new era of image sensing. Within the IR spectra, the shortwave to mid-wave (MWIR) radiations are absorbed by IR photodetectors, whereas the MWIR to very-long wave spectrum is absorbed by IR thermal detectors. Both of these categories of image sensing cover the complete IR spectrum utilized by the applications ranging from bio-sensing in healthcare sector to autonomous vehicle navigation in military and space purposes. Despite having high-cost semiconductor technology with group-II–VI (mercury–cadmium–telluride) and group-III–V (indium–gallium–arsenide) dominating this IR absorbance industry for many decades, the need to have a cost-effective solution has led to an explosion in the exploration of potential materials. Two-dimensional (graphene, dichalcogenides of transition metals, and black-phosphorous) antimonite-based and group-IV/IV alloys have been found to show unprecedented absorption yield and detector properties comparable to traditional dominators with flexible fabrication methods. At the same time, the photon upconversion phenomenon that upconverts low-energy light to high-energy light has emerged as an exceptionally rich area of research in image sensing. The principle behind this concept lies in different energy transfer mechanisms (two photon absorption, triplet–triplet annihilation, cooperative energy pooling, etc.). The advancements that took place most recently in the development of IR absorbers have been reviewed in a concise way. Furthermore, the advancements in upconversion-based detection focusing on how this is evolving as a low-cost alternative for image sensing have been reviewed. Further discussion on how to anticipate a low-power, cost-effective, and light-weight image sensing system has been presented while mentioning some recent research as a proof-of-concept. We finally suggest a possible approach that could come up by synergizing the two simultaneous technologies to foresee the realization of an all-optical, low-power, and light-weight broad-range IR absorber for various applications. © 2021 Society of Photo-Optical Instrumentation Engineers (SPIE) [DOI: [10.1117/1.OE.60.9.090901](https://doi.org/10.1117/1.OE.60.9.090901)]

**Keywords:** infrared thermal detectors; photon upconversion; image sensing; all-optical on-chip photonics; non-linear optics.

Paper 20210686V received Jun. 24, 2021; accepted for publication Sep. 13, 2021; published online Sep. 29, 2021.

## 1 Introduction

Image sensing has undergone a consistent development with advancements in monolithic integrated circuit technology, especially over the last decade. An entire world is hidden in the ranges of light wavelengths that human eyes cannot see. However, today we have entered a new era where infrared (IR) (wavelengths beyond human vision) absorbers can pick up the light emitted from a photosynthesizing plant or a hot battery [by infrared photodetectors (IRPDs)] or even see body heat [(infrared thermal detectors (IRTDS)] to locate enemy forces hiding in the bushes or crossing borders in nighttime (night-vision cameras). The traditional image sensing technology, since World War II, can be broadly classified into two major categories: forward-looking IR and image-intensifier tubes. The commercial low-ambient light cameras up until the last few decades

---

\*Address all correspondence to Anurag Sharma, [anuragsharma.phdece@pec.edu.in](mailto:anuragsharma.phdece@pec.edu.in)

were based on image intensifier tubes (I2Ts). The I2Ts work on the principle of multiplying the low-ambient light in visible- and near-IR light thousands of times. But these could only capture static images and, moreover, suffered from intensity saturation problems (called blooming) due to which they could not be used for real-time operation, which is one of the requirements in today's era of image sensing.

The modern night-vision devices target the applications, viz. surveillance in autonomous vehicles, military surveillance systems for night time operations, searching for resources beneath the earth's crust and beyond our solar systems, faster weather forecasting, and deep-cell tissue detection in bioimaging. These areas have now been diversified into several distinctive fields. All of these applications rely primarily on the emission of radiation by objects in the scene. This is governed by the fact that, for terrestrial temperatures (around 300 K), objects radiate a good portion of the electromagnetic flux as light in the IR part of the electromagnetic spectrum. Typically, night-vision image sensing is based upon IRTD technology.<sup>1</sup> The most common type of thermal detector in IR absorbers/cameras is a bolometer. A very special type of bolometer is widely known as focal plane arrays (FPAs). The FPA technology can be defined as a series of small thin-film bolometers that are arranged in a matrix in the focal plane of the detector. Modern night-vision cameras have achieved the thermal detector absorption capability in the shortwave portion of the electromagnetic spectrum using short-wave infrared (SWIR) absorbers-FPAs that were unused in the military environments. These cameras were able to display real-time images in gray scale similar to I2Ts. One of the research groups developed a technology that can produce full color night vision video in no moon starlight (low-ambience) conditions while at the same time imaging lasers and absorbing IR energy all the way to 1200 nm (SWIR).<sup>2</sup> A wide variety of medical, scientific, industrial, and commercial applications can be realized with such broadband systems. The IRPDs include SWIR absorbers, which can see through smoke and fog and can absorb mid-wave infrared (MWIR/3 to 5  $\mu\text{m}$ ) to long-wave infrared (LWIR/8 to 12  $\mu\text{m}$ ) regions of the IR spectrum, whereas the IRTDs can also see beyond LWIR, i.e., very-long-wave infrared (VLWIR) ranging from 14 to 30  $\mu\text{m}$ . Thus the IR absorbers find many applications in biomedical and thermal imaging, gas sensing, night vision, and spectroscopy mainly due to the high transparency of the atmosphere at these wavelengths that allows for transmission without significant losses. So the authors intend to discuss the growth in recently developed IR absorbers.

The most critical challenges that IR absorbers face are as follows:

1. lowering the fabrication cost,
2. simplifying the fabrication processes,
3. increasing the production yield, and
4. increasing the operating temperature.

The authors further explain the two types of IR absorbers based upon the following principles. The IRPDs consider IR light to be particles, whereas the IRTDs consider IR light to be a heat wave.

- IRPD technologies rely on a light-sensitive material capable of absorbing the electromagnetic radiation reflected from an illuminated object/scene and then converting the absorbed light into an electrical signal that is collected by an on-chip electronic readout circuit.
- IRTD technologies rely on heat wave generated due to the rise in temperature of the object as a result of absorption of light.

IRPDs can have a higher response time and sensitivity, especially for data transmission over C-band/SWIR/NIR (1550 nm), biomedical and thermal imaging, gas sensing, night vision, and spectroscopy. However, a cooling mechanism is required to cut the thermal noise when used at high operating temperatures. The IRTDs are based on semiconductor materials with narrow band gaps (on the order of a few meV, much lower as compared with IRPDs). Over the years, many approaches have been adopted by the research community to enhance performance. One of the approaches is based on engineering the electronic properties of the absorber material to enhance its optical behavior. Another approach relies on increasing the coupling of light to the electronic states of the absorbing material to enable more photons of low-ambient light to be captured and reach the absorber layer. In the last decade, efforts for improving the performance of IRTDs have

been increasing at a faster pace. New concepts such as a wave front imaging sensor with high resolution<sup>2</sup> or multibandpass filters for microbolometers<sup>3</sup> have been developed by engineering the met surfaces to drive this focused research. The key behind these developments lies in high operating temperature, multispectral (or broad-range), IR-FPAs.<sup>4-7</sup> Since most of the conventional IR absorbers were the uncooled type, which requires an additional circuitry for cooling down when operated at higher temperatures, their cost was too high. Thus there was an inevitable need to shift from uncooled absorbers to cooled ones to have a cost-effective thermal image sensing system. By enhancing the detector operating temperatures, reduction in the cost of IR absorber systems has been aimed at, to a great extent, exploration of new material platforms. In the conventional camera system, after the photons of light from a low-ambient scene have been coupled by FPAs and focused on the absorber layer, the electronic readout circuit collects electrical charge carriers generated on applying a suitable bias and guide them in the form of amplified voltage or current to send a video signal to the display electronics. Conventional electronic readout circuits are bulky and complex and have undergone miniaturization with costly on-chip read-out integrated circuits (ROICs).<sup>7-12,13</sup> The FPA captures most of the photons without loss, so nanostructured IR absorbers<sup>14-32</sup> on silicon-based electronic ROIC have been developed. Thus in one of the sections, the authors will describe consistent growth of FPAs based on advanced nanostructures. With a clear focus on portable night vision appliances, any further compaction in size is always anticipated. Also it must be able to work with more battery power, targeting long military operations. The existing electronic-readout circuit is the only portion left in today's image sensing system that consumes maximum power. Hence, the authors identify a need to find a substitute for the electronic-readout portion. This should occur in such a way so as to have a light-weight as well as low-power consuming system for image sensing. The quickest solution that pops up is to go via an all-optical approach, i.e., to have a photonic-integrated readout instead. This is because the growth in on-chip silicon photonics technology has already enabled light-weight, low-power devices for ultra-high-speed data transmission.<sup>33-36</sup> Imagine the scenario of having direct conversion of IR photons to visible photons instead of converting them to excitons (electron-hole pairs) and directing them to a phosphor screen for display. The authors anticipate this possibility of a photonic-readout based on some state-of-the-art concepts. One of them that is focused on in this paper is photon upconversion. Photon upconversion is an anti-stoke criteria (i.e., high-wavelength to low-wavelength conversion). The antistoke materials, viz. rare-earth doped materials (inorganic) and dye-sensitizers, and polymer (organic) materials have promised much better quantum efficiency by being able to collect most of it from available white light in nature. The concept of photon upconversion is a process in which the sequential absorption of two or more low-energy photons leads to the emission of higher energy photon, i.e., emitting light at a shorter wavelength than the excitation wavelength. So the authors will also review the latest achievements in upconversion-based new material developments, further inferring how this may take a new leap toward advancements in broad range-IR to visible image sensing in the future. In the following sections, the focus is to foresee the realization of an all-optical, light-weight, low-power, and broad-range image sensing system for various applications. Section 2 discusses recent works demonstrating progress in IR absorbers, with a focus on thermal detectors for image sensing, with a superior spectral response over the wide IR spectrum. Further, the classification of top contenders in optical material platforms showing tremendous optical properties has been reviewed. In Sec. 3, we discuss current scenario of photon upconversion energy transfer mechanisms and predict the best possibility for anticipating an all-optical image sensing technology platform.

## 2 Infrared Absorbers

IRTDs are one of the two categories of IR absorbers along with IRPDs that are gaining importance in extracting the most from the IR spectrum. Despite the rapid advances of 2D-thin film-based MWIR thermal absorbers enabled by the state-of-the-art CMOS technologies, the current scenario is subjected to the poor stability and difficulty in integrating this at a large scale. Thus it needs a disruptive low-power and economical solution.<sup>37</sup> Some of the latest CMOS technologies developed recently for fabricating such devices are the van der Waals epitaxial growth of a

wafer-scale 2D platinum ditelluride ( $\text{PtTe}_2$ ) layer capable of sensing ultra-broadband light of up to  $10.6 \mu\text{m}$  with a high-specific detectivity.<sup>38</sup> The heterogeneous integration of graphene photo-detectors (PDs) and Si waveguides on  $\text{CaF}_2$  substrates is another CMOS technology that recently demonstrated LWIR waveguide-integrated sensing. It utilized a high-yield transfer printing method, specially developed for flexibly integrating the waveguide and substrate materials to solve the issue of bottom cladding material absorption. The technology managed to show comparatively lower losses in the broad MWIR wavelength range of 6.3 to  $7.1 \mu\text{m}$ .<sup>39</sup> It was later in the 20th century when research in IR absorbers started to develop mature devices for a wide variety of medical, scientific, industrial, and commercial applications. For thermal detection in the MWIR and LWIR regions, having its own place requires strong light-matter interactions using a light-sensitive material with a large absorption capability to capture low-energy photons. This led to the research toward development of nanostructured thin films exhibiting broadband response over the entire MWIR to VLWIR spectrum. Materials with three-dimensional micro- and nanoarchitectures exhibit many beneficial mechanical, energy conversion, and optical properties. However, these three-dimensional microarchitectures are significantly limited by their scalability. Efforts have been successful only in demonstrating overall structure sizes of hundreds of micrometers or containing size-scale gaps of several orders of magnitude. This results in degraded mechanical properties at the macroscale. An ample number of state-of-the-art hierarchical metamaterials has been developed in the last five years, with disparate three-dimensional features spanning seven orders of magnitude, from nanometers to centimeters. The power of these metamaterials is felt in the case of integrated optics while trying to concentrate the electromagnetic energy at precise spatial locations to enable sensing, especially the design of nanoscale 3D metamaterial structures.<sup>40–51</sup> With their feature sizes reaching beyond tens of centimeters, these unique nanostructured metamaterials might find use in a wide area of applications in the Internet of Things. With the availability of fabricating heterostructures comprising thin films being monolithically stacked on each other,<sup>22</sup> a lot of noble solutions by engineering strong light-matter interactions have been developed. As a consequence, the development by engineering nanostructures from higher structural dimensions to zero dimensions started. Further with a focus toward on-chip light sources and light detection devices, a lot of consistent research produced thin films for IR absorbers using a variety of heterostructures topologies. These can be categorized as quantum wells (QWs),<sup>52–54</sup> quantum dots (QDs),<sup>55–59</sup> and quantum dots-in-a-well (QDWELLs),<sup>60,61</sup> these have proved huge spectral tuning capability complimenting the improved absorption of light. Over the last decade, broadly classified thermal detectors have been developed using two basic approaches. The first is based on epitaxially grown structures as mentioned previously or using the narrow band-gap engineering of these nanostructures, especially with the huge advancements in nanostructures for enhanced IR absorption like the development of the very first lead sulfide ( $\text{PbS}$ )-based IR detectors with detection capability up to  $3 \mu\text{m}$  wavelength range. This technology has matured to a great extent, especially over the last decade. The material growth has come a long way from lead selenide ( $\text{PbSe}$ ), lead telluride ( $\text{PbTe}$ ), and indium-antimonite ( $\text{InSb}$ ) to alloying of group (III–V),<sup>58,59</sup> group (IV–IV)<sup>62–67</sup> elements successfully, which caters to the development of a new class of bandgap engineered semiconductor-alloy materials. However, the top materials in the IRPD market due to their band gap tuning capability and highest Shockley–Read–Hall (band-to-band recombination time) lifetime (spanning from SWIR to MWIR) are mercury–cadmium–telluride (MCT),<sup>68–70</sup> mercury–telluride,<sup>58,59</sup> indium–gallium–arsenide<sup>5,71</sup> alloys, and recently antimonite-based materials<sup>11,24</sup> have revolutionized the way of IR detection. This IR absorber material journey has been well explained in some of the works.<sup>11,19,25,26,60,71–76</sup> The authors thus describe the most promising nanostructured developments targeting broad-range IRPDs for MWIR and LWIR wavelengths into broad categories on the basis of epitaxially grown narrow bandgap semiconductors.

## 2.1 CQD Structures

Despite having a mature gallium–arsenide (GaAs) substrate growth and fabrication process as well as high uniformity, QW technology<sup>77</sup> as an independent candidate for broad range IRPDs has begun to lose its importance. The most significant reason is their low-quantum efficiencies at MWIR and LWIR ranges and inability to absorb light at normal incident angles. This leads to

their poor performance at high operating temperature, thus prompting the researchers to look for the next milestone in the nanostructured engineering with multiple quantum well (MQWs) structures<sup>78</sup> and zero dimension structures, i.e., QDs and QDWELL. By incorporating the zero dimension structure disruptively in different material systems, researchers have been able to achieve very high sensitivity to IR irradiation at normal incidence, lower dark current, and higher operating temperatures with longer carrier lifetime. The current research regarding QD-structure mainly focuses on improving its low-absorption quantum efficiency. The problem was solved by self-assembled (colloidal) QDs CQDs. Manis-Levy et al.<sup>79</sup> in a recent work, used thin films of nanocolumnar PbSe for extended SWIR detectors. Such developments prove the importance of the SWIR region, thus leading the way toward low-cost SWIR imaging technology. The growth and the optical and electrical characterization of such PbSe nanocolumnar (NC) layers is actually an advanced version of self-assembled (colloidal) QDs engineered in a different way and grown on a GaAs substrate, where the nanocolumns were laterally separated by grain boundaries rather than by organic ligands as in colloidal QD-based layers. Optical and electrical characterization confirmed the potential of these films as absorber layers for the SWIR range beyond 1.6  $\mu\text{m}$ . CQDs as an emerging class of nanostructures have proved to be the most significant contender for cost reduction in the field of IR optoelectronics. Exhibiting strong interband absorption in the thermal IR range, CQDs can be produced at a low-cost benchtop colloidal synthesis and mated with existing electronic platforms to finally have a cost-effective imaging system. Most of the conventional mercury-based CQDs being incorporated in IR devices are surface bounded, which means that their disposal could lead to serious environmental and health hazards due to the poisonous nature of mercury. Maintaining high detectivity while lowering the cooling requirements, CQDs have proved to be a state-of-the-art methodology. As in conventional devices, the surface recombination (Auger) process shortens the carrier lifetime at high operating temperatures. Thus making it inevitable to use the externally cooled IR absorbers for enabling high performance in cryogenic conditions. Unlike carrier delocalization in bulk films, CQD-films have localized charge carrier generation, which creates different interactions. Hafiz et al. confirmed that having careful engineering of CQD-films with built-in Auger suppression may serve as a potential candidate for the long-desired uncooled thermal detector with low weight, low power, and low cost.<sup>79</sup> Due to the lattice mismatch between substrate and epitaxial layer, the process of self-assembly occurs. The pseudomorph growth process elongates the lattice of the top layer toward growth direction. However, the compressive strain starts to relax after a certain thickness, which is called the critical thickness. The plastic relaxation of strain creates the three-dimensional QDs (colloidal QDs), called artificial atoms. This enables absorption at normal incidence, longer lifetime for excited carriers, and lower carrier–phonon interaction. One major problem in CQDs is inhomogeneity in varying the quantum-dot size distribution, which leads to low-absorption efficiency. To overcome this, Panda et al.<sup>80,81</sup> proposed a strain-coupled bilayer QD structure with a new growth strategy based on homogenous size distribution of QDs from the bottom toward the top QD layers. This was the first reporting of a Bilayer QDIP structure with optimized growth strategy as shown in Fig. 1, which clearly depicts a broad IR response from 3.5 to 8  $\mu\text{m}$ . The intensity ratio of lower wavelength response (3.5 to 5.5  $\mu\text{m}$ ) to higher wavelength response (6 to 8  $\mu\text{m}$ ) increased at 75 K due to the increment in thermionic emission. The device responsivity has been calculated for the wavelength at which the spectral response has the highest intensity ( $\approx\lambda_p = 7.1 \mu\text{m}$ ). Such a device is further expected to have an enhanced response toward the MWIR window (8 to 12  $\mu\text{m}$ ) by optimizing the spacer thickness and the monolayer coverage of the InGaAs dots. However, the maximum absorption quantum efficiency with this kind of structure is  $\sim 18\%$ ,<sup>80</sup> which is better than conventional technology but still needs improvement.

## 2.2 Type II Superlattice Structures

A periodic structure of two or more materials is typically known as low-dimensional structures such as arrays of QDs or quantum wires. This was the basic definition given to superlattice structures before the concept of type-II superlattice structure was introduced by the Nobel laureate Esaki.<sup>80</sup> In 1987, these structures were proposed for IRPDs by Smith and Mailhot;<sup>82,83</sup> thereafter type-II superlattice (T2S) structures have evolved as an efficient solution with higher operating temperature and multispectral response (from SWIR to LWIR) because of

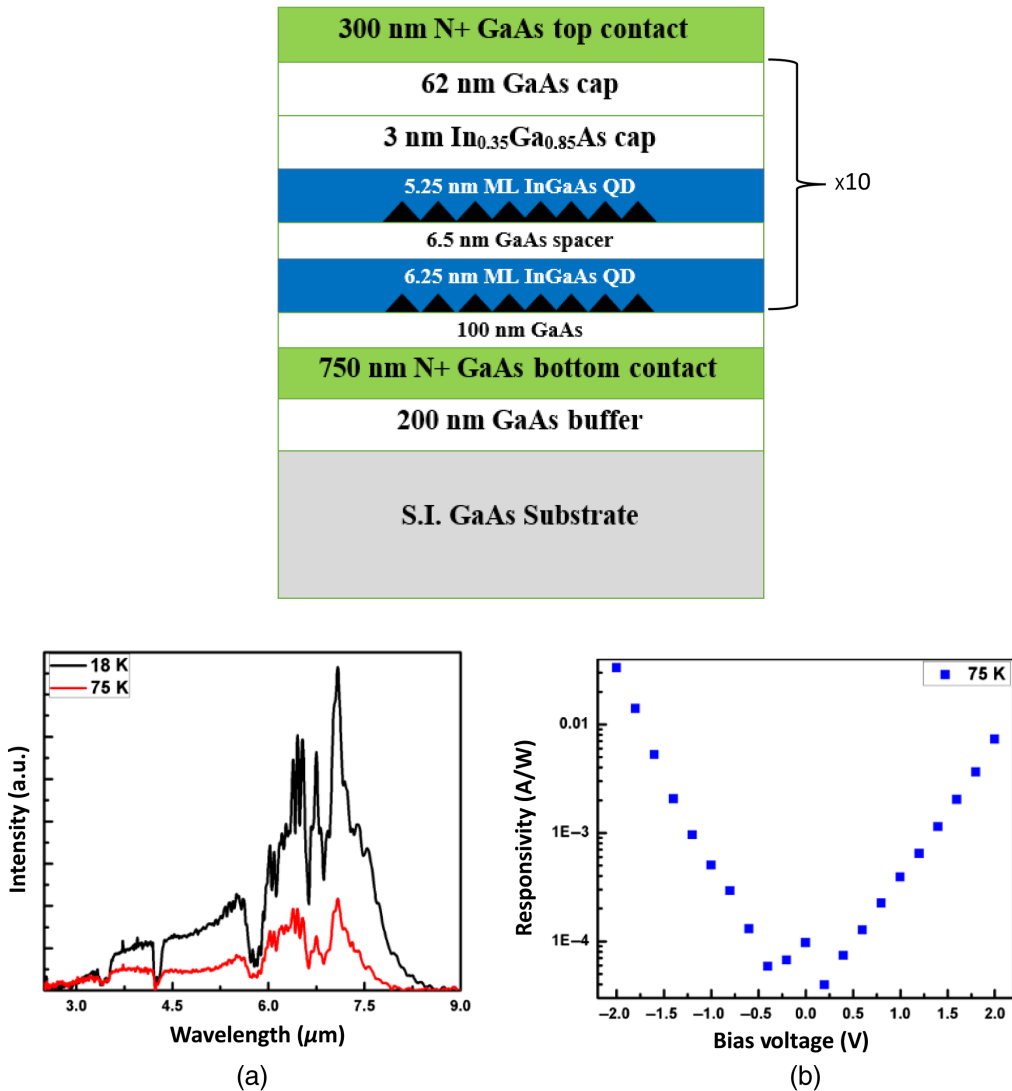


**Fig. 1** Heterostructure of proposed bilayer QDIP: (a) 18 and 75 K spectral response with  $-2\text{ V}$  applied bias and (b) bias-dependent responsivity at 75 K, measured for  $7.1\text{ }\mu\text{m}$ .

its high-absorption coefficient. Figure 2 shows the M-structure superlattice, which has been successfully integrated onto type-II InAs/GaSb superlattice photodiodes; it demonstrates orders of magnitude in improvement for the electrical performance of LWIR and VLWIR absorbers.<sup>84</sup> One of the benefits of the type II superlattice (T2S) is the capability to tune the detection cutoff wavelength over a very wide range. By adjusting the thicknesses of constituent layers, the energy gap of the structure can be precisely controlled with excellent uniformity over a three inch wafer area. One of the research groups experimentally demonstrating the type-II InAs/GaSb superlattice photodiodes with the cutoff wavelength varying from  $3.5$  up to  $32\text{ }\mu\text{m}$ .<sup>85</sup> The measured results fit nicely with the theoretical prediction using the empirical tight-binding model.<sup>86,87</sup> At the longest cutoff wavelength ( $\sim 32\text{ }\mu\text{m}$ ), the detectors have a peak responsivity of  $3\text{ A/W}$  and a detectivity of  $4.25 \times 10^{10}\text{ cm Hz}^{1/2}/\text{W}$  at  $15\text{ }\mu\text{m}$  under  $40\text{ mV}$  reverse bias at  $34\text{ K}$ . Figure 3 shows the growth of IRPD-FPAs based on type-II InAs/GaSb superlattice structures. Subsequently, antimonite-based materials (InAs/GaSb T2S) have also shown to be future prospects as a great competitor to MCT-based T2S structures for broad-range IRPDs due to their comparable Shockley–Read–Hall lifetime.<sup>24</sup> The rate of development in this field would soon be able to overcome its limitations in terms of low yield with the fabrication of large FPAs. Some of these suppressed crosstalk antimonite-based T2S thermal absorber topologies have been developed for dual-band imaging.<sup>88–91</sup> The design shown in Fig. 4 shows an air-gapped distributed

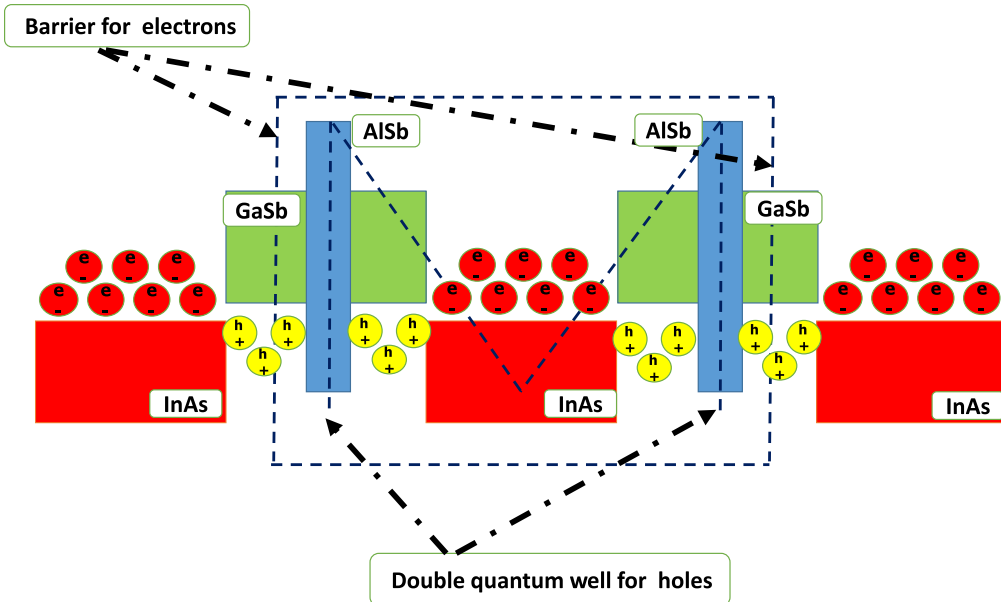


**Fig. 2** Schematic diagram of *M*-structure type-II superlattice structure.

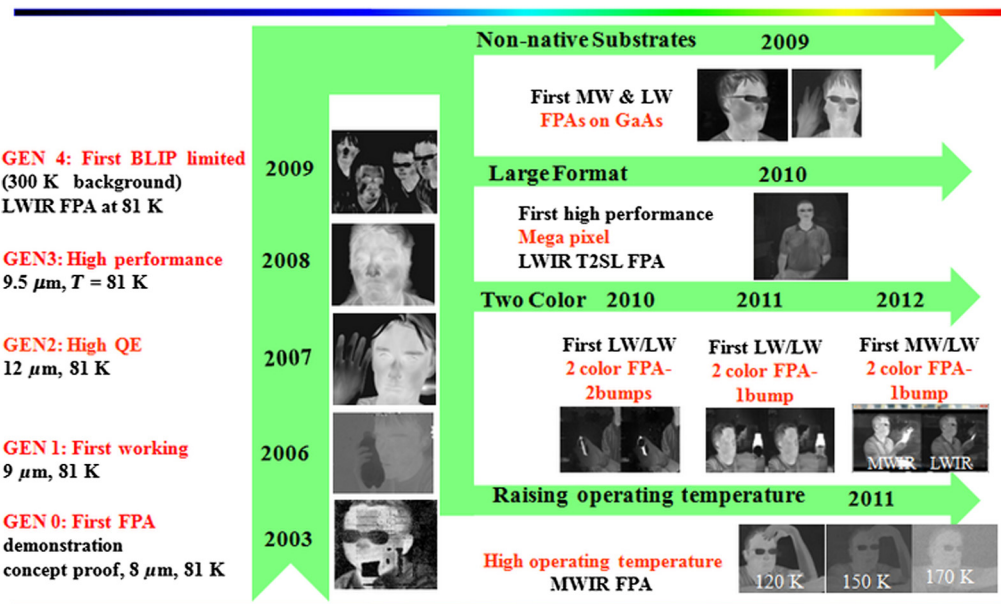


**Fig. 3** IRPD-arrays based on type-II InAs/GaSb superlattice structures.

Bragg reflectors (DBRs) monolithically integrated between the two channels in LWIR dual-band InAs/InAs<sub>1-x</sub>Sb<sub>x</sub>/AlAs<sub>1-x</sub>Sb<sub>x</sub>-based T2SLs PDs. DBRs have a long history covering a lot of applications that require optical filtering to target specific wavelengths.<sup>92</sup> This technology is now being used to suppress the optical crosstalk issue in LWIR dual-band imaging. However, there were challenges that had to be resolved before using DBRs as crosstalk limiters. One was the need to insert a thin layer of Brag-reflector between two channels of a two-color absorber unlike in the case of conventional grating structures. Also the DBR mirror has to be lattice matched to the absorber layer. Thus air-gapped DBRs further anticipate an important milestone toward low-cost multicolor absorption. Enhanced-two-dimensional (2D) structures 2D materials such as graphene and transition metal dichalcogenides (TMDC), due to their high-temperature operability and low-fabrication cost, have emerged as another interesting candidate for desired IR

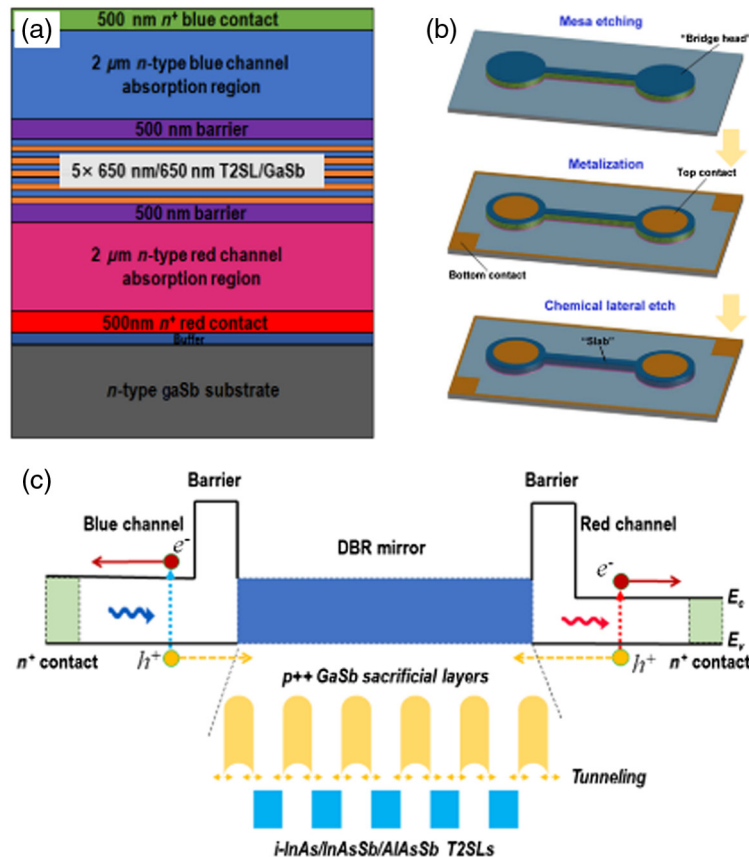


**Fig. 4** Schematic diagrams showing (a) the epi-structure for asymmetrically grown LWIR dual-band PDs and (b) the process flow for fabricating LWIR dual-band PDs with air-gapped DBRs. (c) Schematic diagram and working principle of the dual-band LWIR PDs with monolithically integrated DBR mirrors.

absorption.<sup>93</sup> However, their low-absorption coefficient makes them less sensitive to ambient light, which has been the biggest bottleneck for many years, as reviewed extensively in recently published works.<sup>7,61,94,75,76,95,96</sup> Moreover for large FPAs IR absorbers, the cost factor is too high. By synergizing these efficient materials with new topologies of metasurfaces (such as DBRs and CQDs) and strong light–matter interaction using zero-dimension structures discussed previously, the researchers have succeeded in overcoming the limitations to a great extent. Broadly, the topmost 2D materials that have emerged in the last few years with superior properties for IR absorption over a broad range of spectrum are graphene and black phosphorus (BP). BP has recently been reported in a work outperforming TMDCs.<sup>97</sup>

### 2.2.1 Graphene-based structures

Graphene-based structures have been the most significant milestone in the emerging field of group-IV photonics. This material successfully has been able to complement the silicon platform for developing active photonic devices. Sassi et al.<sup>98</sup> demonstrated an MWIR bolometer type graphene-based uncooled detector with its temperature coefficient of resistance of 4% to 11%/K, as shown in Fig. 5. This technology, when used as MIR PDs, delivered promising performance (in terms of responsivity, speed, and noise equivalent power) even on bulk substrates and were capable of detecting hot bodies in their proximity. Further, spectral selectivity is anticipated by patterning resonant structures as part of the pixel layout. This technology is competitive on a number of levels, ranging from high-resolution thermal imaging (small pixel limit) to highly sensitive spectroscopy in the MWIR and VLWIR (large pixel limit). Here the cooling capability results from the pyroelectric substrate. Overcoming the weak light absorption of low responsivity

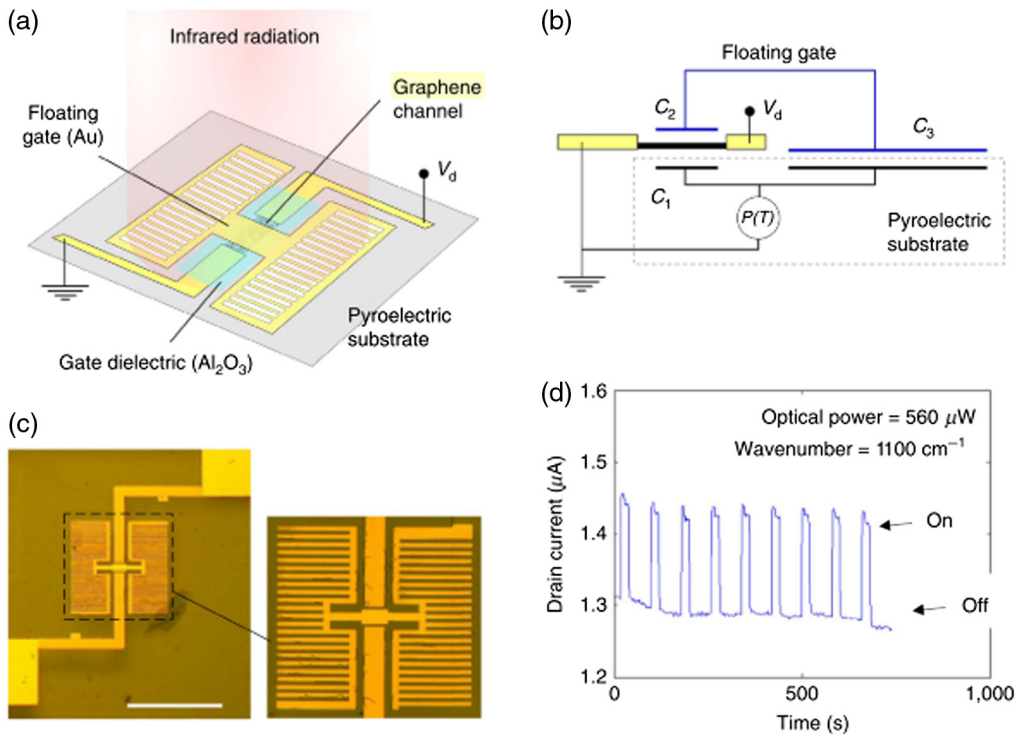


**Fig. 5** Graphene pyroelectric bolometer: (a) scheme of an individual device, where the conductance of a single-layer graphene (SLG) channel is modulated by the pyroelectric substrate and a floating gate. This is driven by two metallic pads in contact with the substrate, with a total area much larger than the overlap with the SLG channel. Such pads can be either uniform or patterned. (b) Circuit diagram for the device in (a). (c) Optical image of a device with lateral pads patterned as electrically connected finger-like structures. Scale bar, 300 nm. (d) Response at  $1100\text{ cm}^{-1}$  ( $\sim 9\text{ }\mu\text{m}$ ) over several ON/OFF cycles induced by a manual shutter. The laser spot size is 300 nm. The drain current is measured for a 10-mV drain voltage ( $V_d$ ).

graphene-PDs, Talebi et al.<sup>20</sup> recently fabricated an MWIR PD from hybrid graphene–PbSe nanorods, which have a fast response with  $\sim 10$  times higher responsivity as compared with conventional nanorod-based detectors. Bansal et al. recently succeeded at having a superior external quantum efficiency, responsivity, and detectivity for VLWIR using a bilayer graphene/MCT IRPD structure, as shown in Fig. 6. They demonstrated a high-performance p+BLG and few layer graphene/n-Hg<sub>0.8133</sub>Cd<sub>0.1867</sub>Te heterojunction VLWIR detector.<sup>68</sup> Such a superior

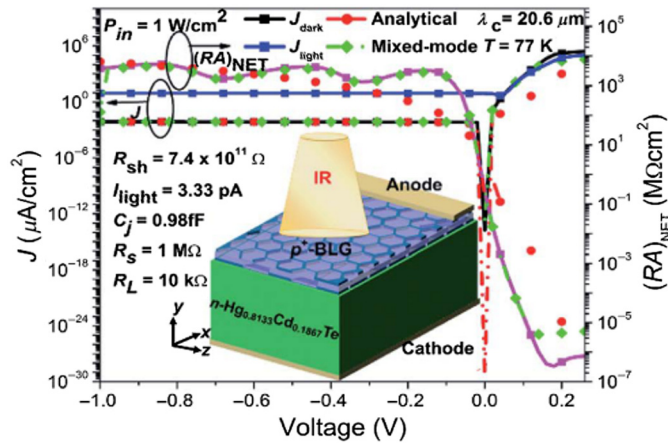


**Fig. 6** The electrical characteristics of p+-BLG/n-Hg<sub>0.8133</sub>Cd<sub>0.1867</sub>Te heterojunction VLWIR PD at a cutoff wavelength of  $20.6\text{ }\mu\text{m}$ .

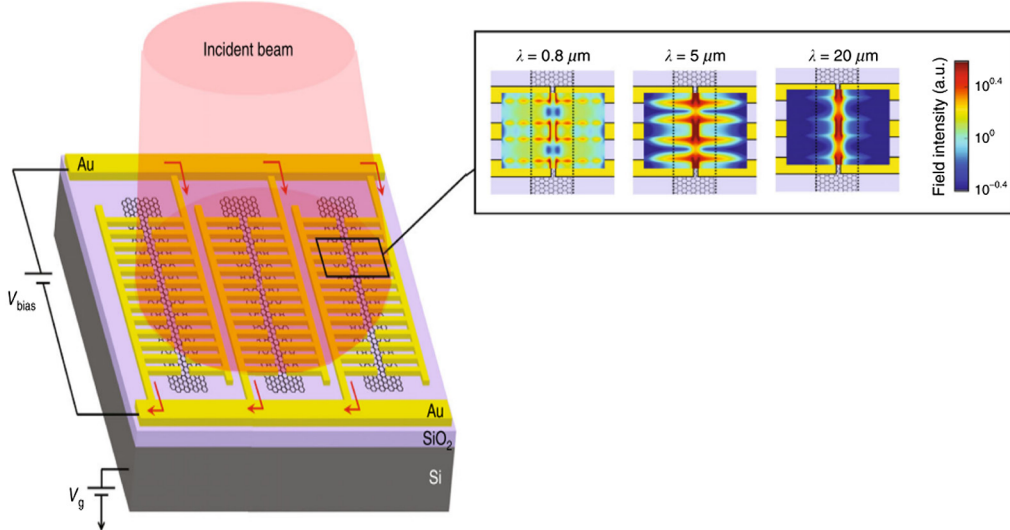


**Fig. 7** High responsivity and broadband photodetection via gold-patched graphene nanostripes.

performance has been attributed to the hot-carrier multiplication mechanism in graphene, which anticipates a huge scope for next-generation high-performance, ultra-low-power, low noise, and cost-effective IR photodetection. Surface plasmons are collective electron oscillations in conducting materials, capable of large optical fields.<sup>99</sup> With a view to efficiently convert the surface plasmons and henceforth their decay into measurable electrical signals with lesser response time to boost the weak-light (low-ambient conditions) absorption by the conventional 2D-materials. Guo et al.,<sup>100</sup> following a history of attempts to enable plasmon-to-electron direct conversions, presented the importance of graphene as a promising platform for MWIR detection and terahertz plasmonic applications by exhibiting stronger light confinement and long carrier lifetime.

This work presented the use of mid-IR plasmonic resonances in discrete graphene resonators combined with quasi-one-dimensional (1D) graphene nanoribbons, with thermally activated carrier transport that is substantially influenced by the plasmonic absorption. Importantly, the device was fabricated on large-scale chemical-vapor deposition graphene, which allows for scalable fabrication, using arrays of plasmonic-resonators interconnected by quasi-1D nanoribbons, rendering it a promising candidate for the development of high-resolution MWIR large-FPAs and high-density integrated IR photonic circuits. Finally, as shown in Fig. 7, Cakmakyan et al.<sup>101</sup> used gold-patched graphene nanostrips (engineered QDs) to design an ultra-fast, high-responsivity, broad-range (from 0.8 to 20  $\mu\text{m}$ ) PD. Covering a range from visible to LWIR is an important breakthrough toward our desired device.

### 2.2.2 Black phosphorus-based structures

Zhou et al.<sup>25</sup> recently discussed developments in the study of BP as an IR absorber, presenting the state-of-the-art synthesis methods for preparing single-layer or few-layer BP methods for characterizing its electronic, optical, and mechanical properties and henceforth developing functional devices. This material has the biggest advantage in terms of its narrow band gap ranging from 0.3 to 2 eV for all thicknesses. With an increase in the number of layers, its bandgap gradually decreases and ultimately reaches 0.3 eV in bulk. Having band-gap tuning (from the visible to MWIR) along with outstanding electrical properties (high hole mobility, high on/off current ratio, and good current saturation), this material is set to overcome conventional material bottlenecks for optoelectronic applications with broadband absorption. Huang et al. realized an integration of silicon-on-insulator (SOI) waveguides with BP PDs. When operating near BP's cutoff wavelength, where absorption is weak, the light–BP interaction is enhanced by exploiting the optical confinement in the Si waveguide and grating structure to overcome the limitation of absorption length constrained by the BP thickness. At a bias of 1 V, the BP PD achieved a responsivity of 23 A/W at 3.68  $\mu\text{m}$  and 2 A/W at 4  $\mu\text{m}$  and a NEP < 1 nW/Hz<sup>1/2</sup> at room

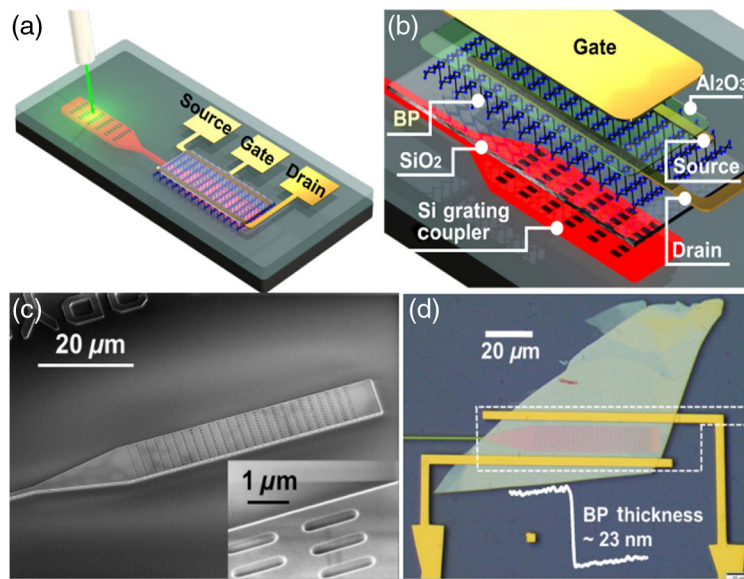


**Fig. 8** Device structure: (a) schematics of the waveguide-integrated on-chip system with BP PD. The light is coupled into the input grating coupler from an optical fiber, transmitted through the waveguide, and coupled into the BP PD by the output grating coupler; (b) zoom-in view of the output side of the device; (c) SEM image of the Si grating coupler, inset: zoom-in image of the grating structure; and (d) microscope image of a BP PD on Si grating coupler before top-gate patterning. White dash line: outline of the top gate; white solid line: AFM height profile of the 23-nm BP flake.

temperature. This integration of passive silicon (Si) photonics and an active BP PD is envisaged to offer a potential pathway toward the realization of integrated on-chip systems for MWIR sensing applications.<sup>25</sup> Figure 8 depicts the device schematics of the waveguide-integrated on-chip system with a BP PD. In addition to the bandgap tuning properties, BP has outperformed silicon in terms of saturation velocity and electric field. This breakthrough was reported by Chen et al., who observed high-intrinsic saturation velocity of  $1.2 (1.0) \times 10^7 \text{ cm s}^{-1}$  carriers at a critical electric field of  $14 (13) \text{ kV cm}^{-1}$  in 7- to 11-nm thick BP for both electrons and holes as a function of charge-carrier density, temperature, and crystalline direction. Compared with another popular 2D layered n-type semiconductor, MoS<sub>2</sub> (a TMDC material), BP outperformed both in saturation velocity and critical field, whereas the transistor off-state current can be larger. With such a high saturation velocity in black-phosphorous thin films at room temperature, the group achieved 2.1 ps of intrinsic carrier transit time in a BP phototransistor with a 250-nm channel length, compared with large photocarrier lifetime ( $\sim 100$  ps), offering great potential for an ultrafast phototransistor with intrinsic photoconductive gain. Such advantages suggest BP as a promising thin-film material for high-frequency transistors, rectifiers, and MWIR absorbers and optical modulators.

### 2.2.3 Emerging SiGeSn structures

The search for effective nanostructured materials started when silicon-photonics (a subset of group-IV photonics) had matured enough to deliver applications within C-band fiber-optic communications. Going beyond the limitations of silicon and germanium, exploration with other group-IV elements started, and researchers found the indirect to direct bandgap tuning by alloying variable tin (Sn) concentrations in SiGe (silicon germanium).<sup>102</sup> Tran et al.<sup>103</sup> successfully developed low-cost SWIR Ge<sub>0.89</sub>Sn<sub>0.11</sub> detectors with a longwave cutoff of  $2.65 \mu\text{m}$  and a responsivity of  $0.32 \text{ A/W}$  at  $2 \mu\text{m}$ , which corresponds to an external quantum efficiency of 20% without any contribution from the Ge buffer layer. The observed specific detectivity of the detector at a temperature of 77 K was only an order of magnitude lower than that of the market-dominating extended-InGaAs photodiode. Following this trend into longer IR ranges, newly

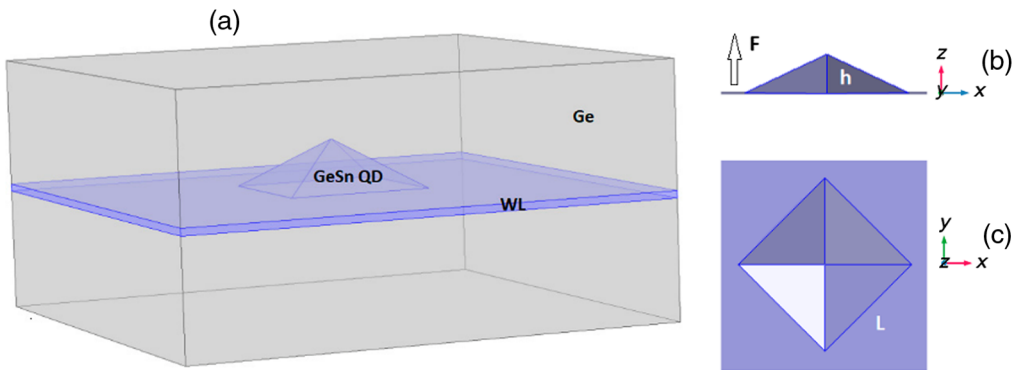


**Fig. 9** Schematic sketch of the pyramidal shaped self-assembled GeSn QD with 1-nm-thick wetting layer (WL): (a) 3D projection of the pyramidal QD with WL, (b) cross-sectional view ( $ZX$ ) showing the QD height and the direction of the external electric field, and (c) plane view ( $XY$ ).

developed  $\text{SiGe}_{1-x}\text{Sn}_x$  alloys was also reported in the development of a MWIR light emission device.<sup>103</sup> Further, thin-film alloys of  $\text{Ge}_{1-x}\text{Sn}_x$  based on virtual substrate approach<sup>104</sup> have brought the attention of worldwide researchers complementing on-chip photonic applications. Over the last decade, the alloy has emerged as a strong direct-bandgap material showing enhanced photoluminescence over the IR spectrum. Some of the works have found that, with an increase in Sn concentration, both the index of refraction and the absorption coefficient increased to larger values at longer wavelengths. In particular, with 15% to 27% of Sn in germanium–tin (GeSn) thin-film alloys with thicknesses from 42 to 132 nm, samples confirmed an absorption spectral range of 0.190 nm to 6  $\mu\text{m}$  when characterized by variable angle spectroscopic ellipsometry measurements.<sup>105</sup> Such technology developments realize that low-cost group-IV photonics-based active devices can be a huge milestone in overcoming the limitations of traditional IR absorbers. Therefore, understanding the physics of QW structures for GeSn-alloys becomes inevitable. Pareek et al. analyzed the performance of group-IV-based intersubband-QW IRPD with a direct band-gap  $\text{Ge}_{1-x}\text{Sn}_x$  active layer.<sup>106</sup> Following this trend, the research community has also started to explore strong carrier confinement in self-assembled quantum dot (CQD) structures of GeSn-alloy as shown in Fig. 9.<sup>106</sup> The self-assembled structure in Fig. 9 was evaluated for different QD sizes. The performance was validated in terms of intersubband optical transitions, dipole moment, photon absorption coefficient, and refractive index changes with respect to the applied electric field. In this work, the intersubband transition energy and dipole moment were found to be strongly affected by the induced electric field. Another finding was that QDs with larger sizes were observed to be more sensitive. The author briefly presents the most recent developments in IR absorbers, specifically mentioning the design details, and describe the methodology used for enhancement of optical coupling onto the detector layer in Table 1. Some of these works, with a focus to cover the entire IR range of importance, are shown in Table 1.

### 3 Photon Upconversion Mechanisms for Infrared Imaging

IR light contains very low-energy photons. Although the technology is highly matured to collect high-intensity photons having low frequency, for the case for low-intensity and high-frequency photons, the current state-of-the-art is premature.<sup>107</sup> So the mechanism of frequency conversion has been a topic of research interest for some time. In fact, the use of organic dyes<sup>108–117</sup> and ligands of polymers<sup>118–122</sup>-based nanocrystals (NCs)<sup>118,123–125</sup> for converting the photons of light from the target to the desired wavelengths is well known in myriad of commercial applications, viz. fluorescent lamps, lasers, white light-emitting diodes, and displays. This intriguing class of materials with rich energy level configurations, as well as controllable electronic transitions<sup>126</sup> within both inter- and intraenergy levels, is capable of achieving emissions with wavelengths covering the ultraviolet (UV), visible, and IR. A broad classification of the most commonly used upconversion nanoparticles (UCNPs) is summarized in the chart shown in Fig. 10. Sangwan and Hersam<sup>126</sup> found a simple way to enable SWIR vision using the concept of upconversion

**Table 1** Comparison of some recent nanostructured IRPDs anticipating cost-effective technology.

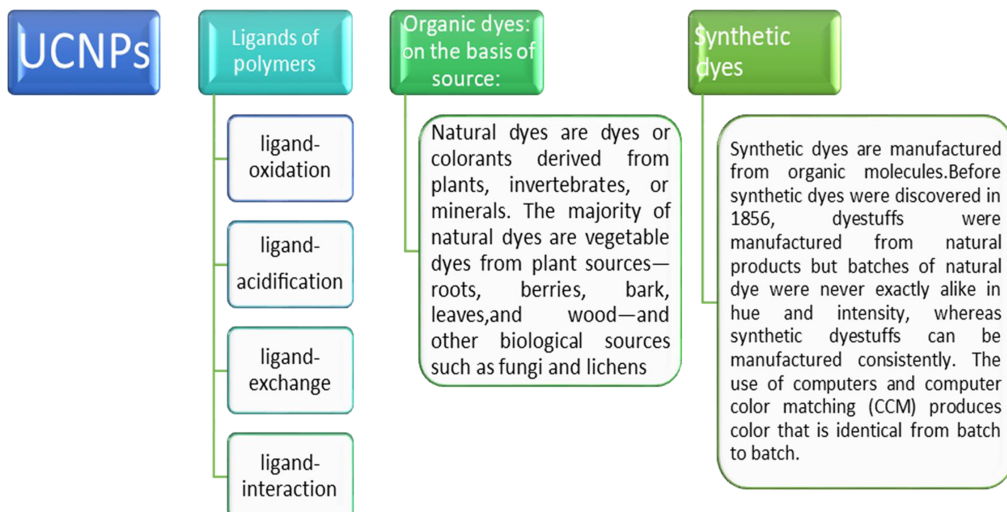
Recent works	Design details	Wavelength range	Nanostructure topology	Material platform	Responsivity		Design details
					Figure of merit	Recent works	
(Campbell et al., 2003) <sup>107</sup>	Wavelength tunable (via capping layer) IRPDs	MW/IR 3 to 5 $\mu\text{m}$ , LWIR 8 to 12 $\mu\text{m}$	QD	n-i-n InAs QDIPs with unintentionally doped active regions	1.3 to 4.11 mA/W	$1.4 \times 10^9 \text{ cm Hz}^{1/2}/\text{W}$	—
(Strassler et al., 2010) <sup>108</sup>	Resonant-cavity enhanced IRPD	MW/IR 3 to 5 $\mu\text{m}$	Thin film over silicon platform	PbTe as absorption layer	100 V/W at 3.5 $\mu\text{m}$	$0.72 \times 10^9 \text{ cm Hz}^{1/2}/\text{W}$	—
(Yakimov et al., 2017) <sup>109</sup>	PD enhanced by surface plasmons	MW/IR peak wavelength = 4 $\mu\text{m}$	QD	SiGe alloy (with 18% Ge) on Ge-substrate	40 mA/W	$1.4 \times 10^{11} \text{ cm Hz}^{1/2}/\text{W}$	—
(Yakimov et al., 2018) <sup>110</sup>	2D plasmonic structures, a gold film perforated with a subwavelength hole array and a periodic lattice of gold disks for IRPDs	MW/IR peak wavelength = 4.2 $\mu\text{m}$	QD	SiGe alloy (with 18% Ge) on Ge-substrate	At reverse (1.2 V) and forward (+1.2 V), $R_p$ correspond to 0.42 and 0.12 A/W	$4.5 \times 10^{12} \text{ cm Hz}^{1/2}/\text{W}$ at 4.2 $\mu\text{m}$	—
(Perez et al., 2018) <sup>111</sup>	Barrier structure with an active zone	MW/IR peak wavelength = 5 $\mu\text{m}$ at 150 K	Type-II superlattice	Ga-free InAs/InAsSb	—	—	—
(Delmas et al., 2019) <sup>112</sup>	Barrier structures in XBP configuration	LWIR peak wavelength = 11 $\mu\text{m}$ at 77 K	T2S	InAs/GaSb	*Quantum efficiency = 60% with antireflecting coating	*Dark current density = $4 \times 10^{-4} \text{ A/cm}^2$	—
(Xu et al., 2019) <sup>113</sup>	Photodiode monolithically integrated on Si	MW/IR peak wavelength = 2 $\mu\text{m}$ (1.6 to 2 $\mu\text{m}$ )	MQW	GeSn/Ge	$\sim 1 \times 10^{-2} \text{ A/W}$ at -1 V	*(Lowest leakage density of 44 mA/cm <sup>2</sup> )	—

**Table 1** (Continued).

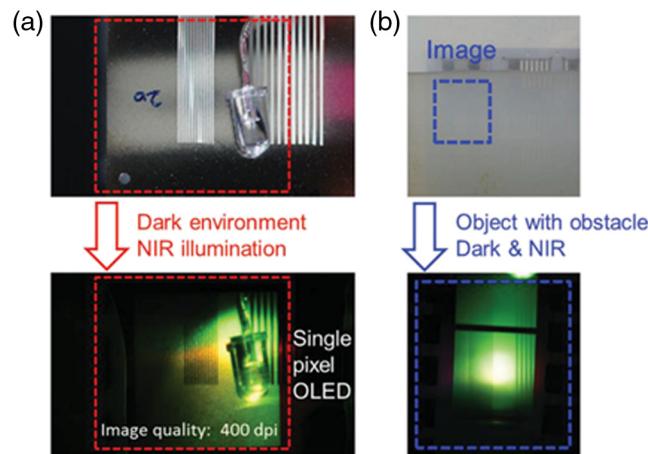
Recent works	Design details	Wavelength range	Nanostructure topology	Material platform	Responsivity	
					Figure of merit	Recent works
(Muller et al., 2018) <sup>84</sup>	Immersion lens technology for optical coupling	LWIR peak wavelength = 10 $\mu\text{m}$ at 200 K	Type-II superlattice	InAs/GaSb	—	$6 \times 10^9 \text{ cm Hz}^{1/2}/\text{W}$
(Pareek et al., 2017) <sup>106</sup>	GeSn heterostructures with 17% Sn composition	Infrared spectrum	Interband MQW	SiGeSn/Ge Sn	8.6 mA/W at 17% Sn-content in GeSn	—
(Gassensq et al., 2013) <sup>106</sup>	GeSn on SOI waveguide integrated PDs	SWIR (0.75 to 2.4 $\mu\text{m}$ ) peak wavelength = 2.2 $\mu\text{m}$	QW	Ge0.9Sn0.1/Ge heterostructure	0.1 A/W for 5 V	—
(Pham et al., 2016) <sup>106</sup>	Normal incidence, double heterostructure	SWIR wavelength = (1 – 2.6) $\mu\text{m}$	QW	Ge/GeSn/Ge with 7 to 10% Sn	0.8 A/m at 1.55 $\mu\text{m}$	$4 \times 10^9 \text{ cm Hz}^{1/2}/\text{W}$
(Wung et al., 2017) <sup>114</sup>	Floating-gate GeSn-heterojunction photoreceivers	SWIR (beyond 2.003 $\mu\text{m}$ )	Heterojunction phototransistor	Ge0.935Sn0.065	~1.8 A/W at 1550 nm and ~0.043 A/W at 2003 nm	*Low dark current density of 0.147 A/cm <sup>2</sup>
(Tran et al., 2019) <sup>115</sup>	Surface passivation technique based-PDs	MWIR peak wavelength = 3.56 $\mu\text{m}$	QW	Si-based GeSn (Sn compositions ranging from 10.5% to 22.3%)	3.2 mA/W for 22.3% Sn compositions	—
(Xu et al., 2019) <sup>116</sup>	High-speed photodetection	SWIR transmission 2 $\mu\text{m}$	MQW	GeSn/Gep-i-n photodiode	—	—
(Ghafari et al., 2019) <sup>117</sup>	Ring-shaped MQWs-based IRPDs	Long-infrared and far-infrared regimes	MQW	GaAs/Al <sub>0.25</sub> Ga <sub>0.75</sub> As	—	10 GHz

**Table 1** (Continued).

Recent works	Design details	Wavelength range	Nanostructure topology	Material platform	Responsivity	
					Figure of merit	Recent works
(Bansal et al., 2018) <sup>117</sup>	Bilayered graphene superlattice based-PD	V/LWIR	Superlattice	Graphene/HgCdTe	Internal = 13.36 A/W at 77 K External = 99. 49% at 77 K, internal = 89%	*Quantum efficiency = 36.16 GHz at 77 K, 129 GHz at 256 K
(Cakmakyan et al., 2018) <sup>101</sup>	Gold-patched graphene nanostripes for broadband and ultrafast photodetection with high responsivity	visible to infrared regime	without the use of bandwidth limiting and speed limiting QDs, defect states, or tunneling barriers	Gold patched graphene nanostripes	(0.6 A/W at 0.8 $\mu$ m and 11.5 A/W at 20 $\mu$ m)	Operation speeds exceeding 50 GHz
(Sassi et al., 2017) <sup>101</sup>	Thermal detectors (pyroelectric bolometers) with temperature coefficient of resistance (411%/K)	MWIR	floating metallic structure that concentrates the pyroelectric charge on the top gate capacitor of the graphene channel	Graphenebased	$2 \times 10^4$ A/W	—
(Zhang et al., 2019) <sup>22</sup>	Dual-band thermal imagers	Dual-band LWIR 7.5 to 11.5 $\mu$ m	Type-II superlattice monolithically integrated air-gapped DBRs	InAs/InAs <sub>1-x</sub> Sb <sub>x</sub> /AlAs <sub>1-x</sub> Sb <sub>x</sub>	2 A/W	*32.4% quantum efficiency
(Zavala-Moran et al., 2020) <sup>118</sup>	LWIR PD	MWIR 4.9 $\mu$ m	Type-II superlattice barrier detector	Free InAs/InAs Sb type-II superlattice	*Dark current density $3.24 \times 10^{-5}$ A/cm <sup>2</sup>	*~35% quantum efficiency
(Shen et al., 2021) <sup>119</sup>	MWIR PD	MWIR 8.3 $\mu$ m	Quantum cascade detector	Ge or Ge-on-Si substrate Ga	0.56 mA/W	$1.5 \times 108$ cm Hz <sup>1/2</sup> /W

**Fig. 10** A broad classification of most commonly used UCNPs.

imaging. Marking the potential of biointegrated NPs for IR applications such as security surveillance in military or even in bioimaging, Han said that, in the future, there may be room to improve the technology with a new version of organic-based NPs that could lead to an even brighter IR vision. This milestone has a long background research history, some of which are mentioned below. This series of developments as a proof-of-concept led to the invention of low-cost bioinspired cameras using both organic (dye sensitizers and ligands of polymers) as well as inorganic (rare-Earth doped) materials. Liu et al.<sup>127</sup> demonstrated a transparent and all-organic-based upconverter converting SWIR (NIR) to green emission in a dark environment and under SWIR illumination. Here using a highly efficient SWIR-absorbing charge generation layer, the upconverters were found to exhibit very high sensitivity to SWIR illumination. They further observed a 3D-image of a real object captured by a digital camera as the first demonstration of its kind using a reflective (metal) and non-reflective (LED) object, as shown in Fig. 11, which indicates its potential in the field of advanced night vision technology. A few years later, Dimitriev et al.<sup>128</sup> demonstrated a broadband upconversion of SWIR in films of organic infrared dye (IR dye). IR dye, with its unique ability to form both J- and H-aggregates in the condensed states, thus plays the role of sensitizer and annihilator, respectively, within which the energy transfer occurs involving dark states as well. Since one of the aggregate serves as a broadband

**Fig. 11** (a) Picture of the line-shaped shadow mask and LD in night vision. (b) Picture of the line-shaped shadow mask when an obstacle (waste water filled cloudy box) was placed between the mask and the camera. SWIR illumination and OLED emission passed through the ITO glass substrate and transparent cathode, respectively.

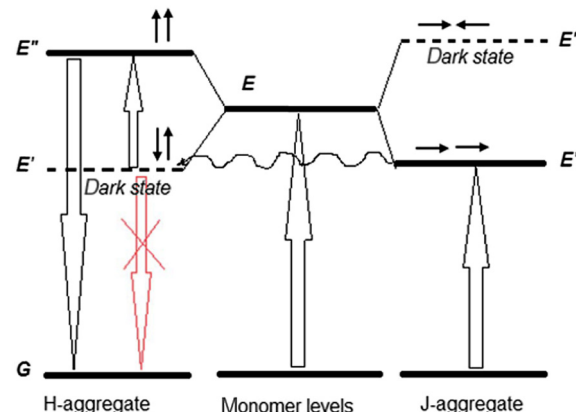


**Fig. 12** The energy transfer mechanism involved in the dye-sensitized upconversion process.

absorber (from ~700 to 1000 nm) and the other as a broadband emitter (from ~450 to 700 nm). This opens up a new perspective for advanced IR to visible light imaging techniques. Figure 12 represents the energy transfer mechanism involved in the upconversion process. In another work by Zheng et al.,<sup>129</sup> some of the unique features of radiative energy transfer upconversion (RETU) proven beneficial for sensing applications were demonstrated in NP-sensitized  $\text{CsPbX}_3$  perovskite quantum-dots (where X = Cl, Br, and I). Figure 13 represents the schematic representation of the RETU processes in all-inorganic  $\text{CsPbX}_3$  perovskite quantum dots (Pe-QDs) through sensitization by lanthanide-doped NPs (inorganic). Lanthanide-doped NPs function as the energy donor to convert the SWIR excitation light into the UV and visible emission light through successive photon absorption and energy transfer upconversion processes within lanthanides. The emission light from the NPs is then reabsorbed by Pe-QDs to create electron–hole pairs (excitons) in the conduction band and valence band, followed by photon emission through excitons recombination. The solid and dashed lines represent the electronic transitions. Similar techniques<sup>120,124,130–135</sup> were found to be much more efficient than conventional multiphoton techniques via effective use of physically existing intermediate energy levels of Lanthanide ions and thus can be triggered by a low-cost NIR laser diode. Another advantage of RETU is the unique photoluminescence lifetime of the excitons that helps in distribution of a large number of excitons over a broad spectra, which proves to be extremely beneficial for time-gated photoluminescence biosensing. Still there is a significant room for improving the stability, toxicity, and upconversion efficiencies of Pe-QDs. The concept has already taken a step toward highly efficient, multicolor photon upconversion in Pe-QDs due to larger carrier lifetimes under low-power density excitations. A further exploration of the concept in synergy with other recent

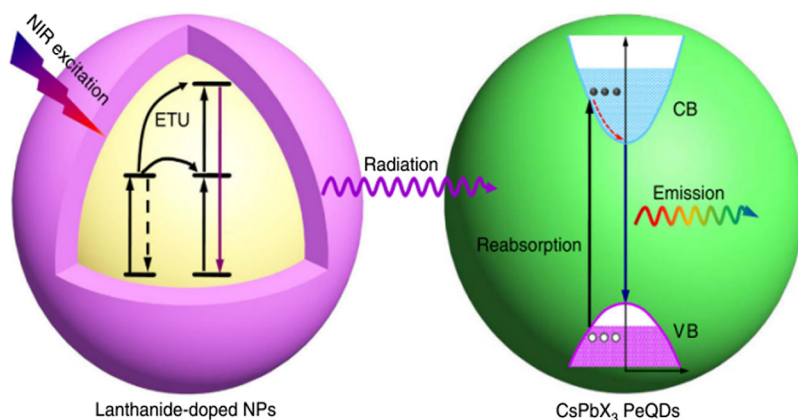


**Fig. 13** Schematic representation of the RETU processes in all-inorganic  $\text{CsPbX}_3$  PeQDs.

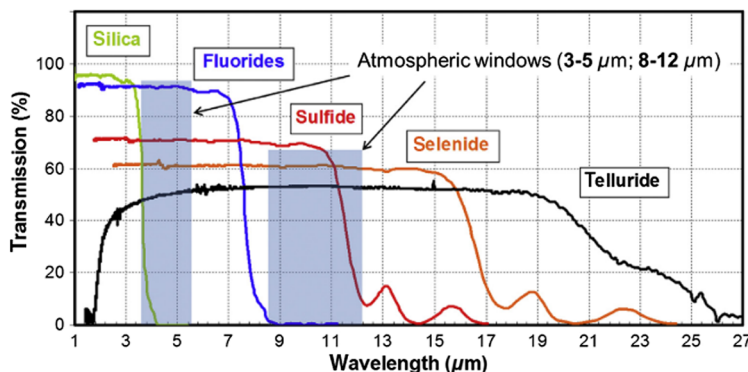


**Fig. 14** Transmission range of different IR glasses.

schemes<sup>123,128,134,136–139</sup> could take a leap toward broadly tuned IR to visible upconversion for high-resolution compact image sensing devices. In another article by Zhang et al.,<sup>114</sup> the advancements in sensing applications based on UCNPs have been reported. It mentions the critical challenges to be addressed in the near future for multidisciplinary research focusing on realizing practical image systems. In this series, one of the major challenges to having a high-peak emission along with the ability to cover a broad IR spectrum was addressed by Du et al. It incorporated GST ( $\text{Ge}_2\text{Sb}_2\text{Te}_3$ ), which is a non-volatile phase change material, to enable wavelength tunability for MWIR thermal emitters using low cost, easy to fabricate layered structures.<sup>140</sup> Aiming at high-peak emissivity over a wider spectrum of IR wavelength, an aluminum (Al) film and an ultrathin (5 nm) top chromium (Cr) film are adopted for these two structures, respectively. The gradual phase transition of GST provides a broad range between 7 and 13  $\mu\text{m}$  while maintaining high-peak emissivity (>0.75 and >0.63 for the GST-Al and Cr-GST-Au emitters, respectively). This study shows the capability of controlling the thermal emission wavelength, the application of which may be extended to gas sensors, IR imaging, solar thermophotovoltaic, and radiative coolers. Zhang et al.<sup>141</sup> reviewed the capabilities of fluoride and chalcogenide glass families as a fantastic material to see beyond visible in the beginning of this decade. This can be observed in Fig. 14, which indicates that selenium (Se) or tellurium (Te) glasses cover the important atmospheric absorption windows. The article concludes that, in the family of chalcogenide materials, only the sulfur-doped glasses have superior transparency in the visible light. Further these inorganic transparent materials are envisaged to collaborate with organic materials to take a leap toward the desired image sensing systems. In another work, He et al. demonstrated a pixel-less imaging chip simply made using a large area single tandem organic upconversion<sup>142</sup> device, as shown in Fig. 15. The tandem organic SWIR-to-visible upconversion devices provide a promising alternative technology for future low-cost, large-area, and pixel-less imaging applications. Further, Fig. 16 represents the use of PbS colloidal NCs as an attractive alternative to existing molecular sensitizers, due to their small exchange splitting, wide wavelength tunability, broadband IR absorption, and efficient energy transfer that was observed by Wu et al.<sup>143</sup> It was later utilized in another work that demonstrated the triplet-triplet annihilation upconversion from NIR (785 nm) to visible (yellow, centered at 570 nm) regions.<sup>144</sup> The advanced night vision devices today need to be much more portable and lightweight, and most importantly have wide tunability over a broader range of the IR band. The MWIR band covers most atmospheric objects with good transmission. Henceforth after having existing proof-of-concepts demonstrated in the recent decade for SWIR-to-visible upconversion-based image sensing devices, the synergy with advanced organic thin films will be the next leap to develop advanced image sensing devices. Another work by Yu et al. showed that bilayer  $\text{PtSe}_2$  combined with defects modulation possesses strong light absorption in the MWIR region and hence they realized an MWIR photoconductive detector operating in a broadband MWIR range. This paved the way for atomically thin 2D noble metal dichalcogenides to be employed in high-performance MWIR optoelectronic devices.<sup>145</sup> Following this trend, a surplus development occurred in the field of upconversion-based detectors (UCDs) capable of absorbing and upconverting IR peaks to visible, directly paving the way toward all-optical image sensing systems.<sup>134,146–153</sup> Table 2

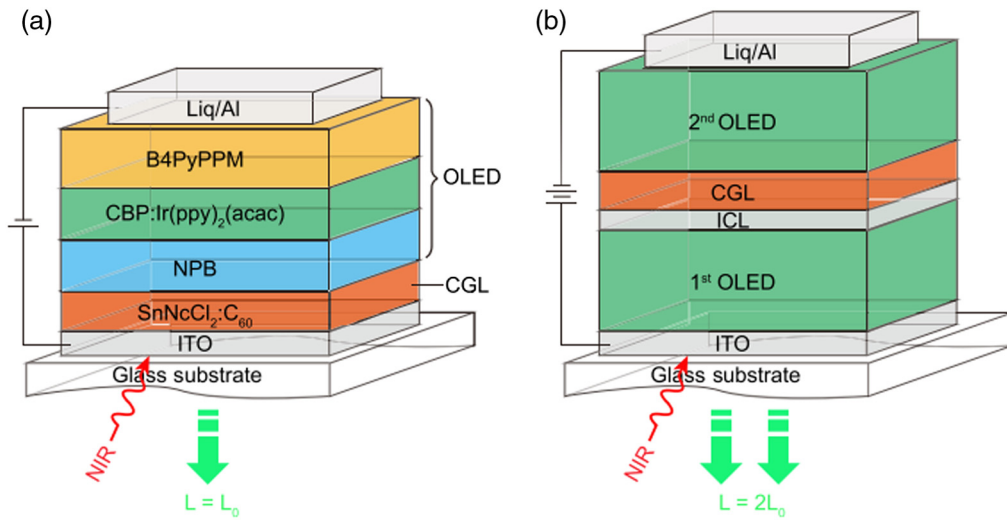


**Fig. 15** Schematic structure diagrams of (a) a conventional organic upconversion device with one OLED unit and (b) a tandem organic upconversion device with two OLED units.

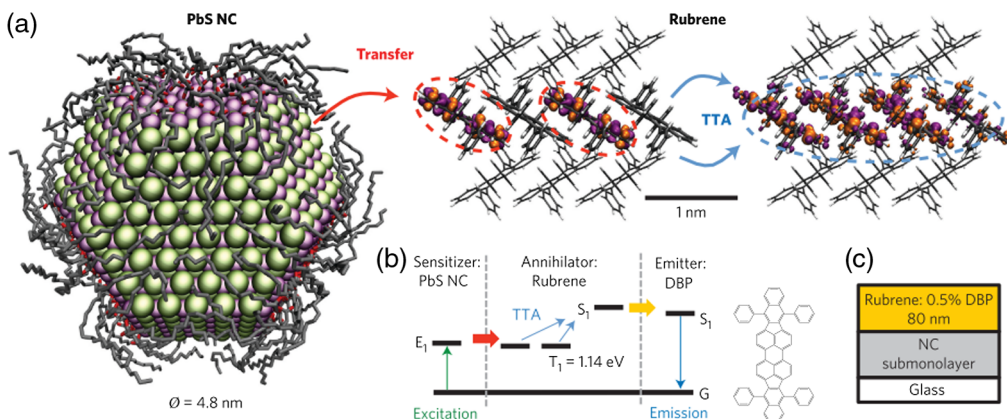


**Fig. 16** Schematics of NC-sensitized upconversion via triplet–triplet annihilation. (a) PbS colloidal NCs absorb incident light and transfer of the energy to the triplet state of neighboring molecular rubrene. If two triplet excitons in rubrene subsequently collide via diffusion, a singlet exciton can be formed. Individual triplet excitons are circled in red, and the larger, delocalized, singlet exciton is circled in blue. (b) Schematic energy diagram showing the processes of triplet sensitization by the NCs, triplet–triplet annihilation in rubrene and emission from DBP. The addition of the DBP (molecular structure shown) as a guest in the rubrene host increases the fluorescence by a factor of 19. (c) The solid-state device structure (not to scale).

presents a comparison of some recent UCDs in terms of their quantum yield and upconversion efficiency as well as material platforms. In addition to deploying schemes such as temperature tuning of the non-linear crystal, using a chirped-poled crystal, sweeping the pump wavelength, using a multichannel wavelength configuration, or using a resonant-cavity enhancement to achieve ultra-broadband response,<sup>154</sup> there exists a huge scope of improvement in acceptance bandwidth as well as upconversion efficiency so as to finally enable a low-cost, multispectral IR UCDs. This section describes the normal structure of a manuscript and how each part should be handled. The important thing to mention is that, among most of these works, those applicable to label-free bioimaging are based upon fluorescence radiative decay mechanism,<sup>155–160</sup> while for thermal imaging we need phosphorescent radiative decay<sup>161–166</sup> with enough time to capture the low-energy photons and thus quickly upconvert them to visible. Most of the development has contributed to the former type of irradiance, enabling low-cost bioimagers, while the latter mechanism still needs transformation from bulk optics to on-chip technology. The research

**Table 2** Comparison of some recent UCD-based topologies in terms of their quantum yield and upconversion efficiency.

Recent works	Application targeted design	Absorbed spectra	Up converted/ emitted spectra	Material platform	Figure of merit	
					Quantum yield	Upconversion efficiency
134	Miniaturized devices can be applied to deep tissue light stimulation or therapy	838 nm (SWIR)	630 nm (red) and 590 nm (yellow) visible light	GaAs (absorption), Ga0.5In0.5P for red emission, Al0.15Ga0.35In0.5P for yellow emission, with AlGaNp-based DBR coating on top	~1.5%	—
171	Low-cost thermoelectric-cooled MWIR imaging cameras	2.2 to 4.2 $\mu\text{m}$	0.84 $\mu\text{m}$	InAsSb/GaSb PD with a GaAs/AlGaAs light emitting diode	—	0.06 W/W at 200 K at 5 V bias
147	Biosensors applications	10.6 $\mu\text{m}$	1.55 $\mu\text{m}$	OP-GaAs avalanche PD with PPLN material for upconversion	~20%	—
136	Single-photon sensitive imaging device based on an intracavity design	3 $\mu\text{m}$	0.785 $\mu\text{m}$	20-mm-long MgO:PPLN non-linear crystal intracavity	~20%	—
154	Ultra-broadband mid-wave-IR applications in biomedical imaging, surveillance systems	3.6 to 4.85 $\mu\text{m}$	820 to 870 nm	20-mm-long periodically poled MgO-lithium niobite crystal in a compact intracavity	~20%	0.08 W/W
139	Broadly tunable upconversion detection	9.4 to 12 $\mu\text{m}$	956 to 977 nm	AgGaS <sub>2</sub> crystal and quantum cascade laser (QCL) pumping	—	—
150	Upconversion raster microscope for imaging of microcalcifications	LwIR 11.11 to 12.5 $\mu\text{m}$	958 to 976 nm	A novel upconversion raster scanning microscope with QCL for illumination and AgGaS <sub>2</sub> crystal	—	—
172	Miniature SWIR light transducers for color night vision	SWIR 980 nm	Visible 535 nm	ocular injectable photoreceptor binding UCNPs which anchored on retinal photoreceptors	—	—
127	An all-organic SWIR upconversion device (AUC)	SWIR 1020 nm	1008 to 1014 nm	An organic SWIR sensitive PD and an organic light emitting diode (OLED), connected in series	—	30%
122	Luminous CdSe/ ZnS QDs	SWIR 980 nm	Visible 535 nm	Solution processed optical upconversion PDs	>80%	6.5% at a low turn-voltage of 2.5 V

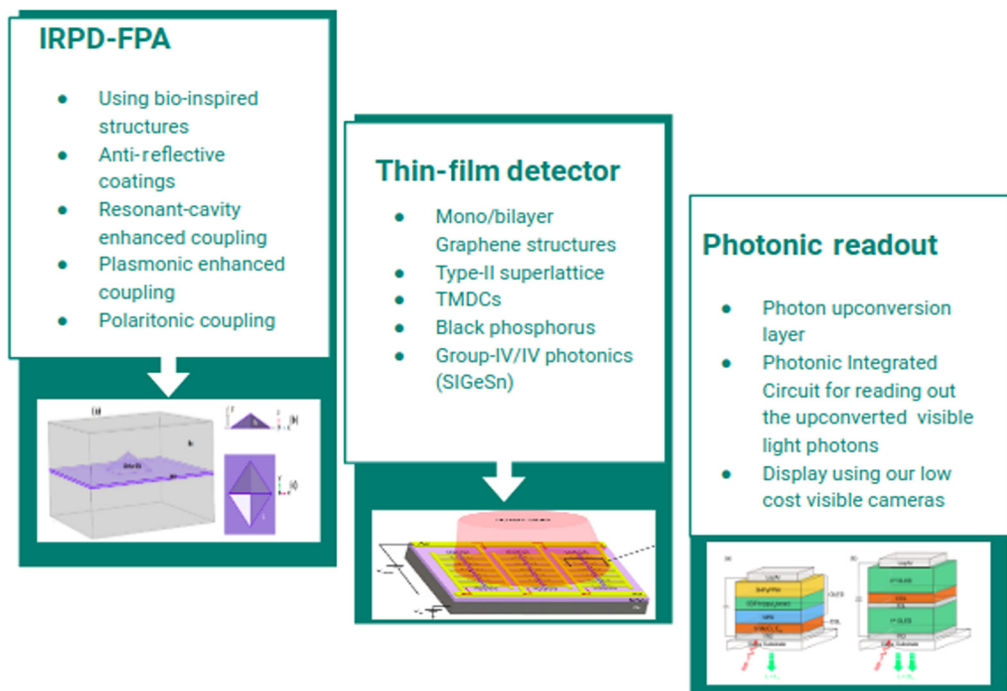


**Fig. 17** A proposed methodology for all-optical system for image sensing.

community has thus accelerated in recent years to create IR image vision with negligible side effects. State-of-the-art technologies that have been developed so far anticipate the possibility of designing a multicolor vision light-sensitive UCNPs as well as advanced bandgap-engineered materials. Furthermore, for visual repair and enhancement, lattice matched NPs can be engineered for enhanced light absorption beyond SWIR. A systematic and careful study is needed of the hour focusing on synergizing upconversion detectors based on periodically poled lithium-niobite structures or lanthanide-doped core/shell architectures with more advanced metasurfaces and zero-dimension quantum structures as mentioned in Sec. 2 to explore the hidden potential of this niche area. The authors thus provide in Fig. 17 a design methodology to move toward an all-optical imaging system-on-chip with cost-effective constraints. Based upon the review, the possibilities toward wider IR absorption have been shown using nanostructured-FPAs above the detector stack. The concept is based on using enhanced optical coupling methods such as resonant cavity enhancement, plasmon-enhanced, distributed-brag gratings, and other bioinspired antireflective structures. The detector stacks based on advanced materials as discussed in Sec. 2 with maximum quantum yield have to be carefully selected. Now once the low-energy (IR) photons have been captured from low-illuminated ambient surroundings, instead of converting them into phonons (electron–hole pairs) and creating images using a costly CMOS electronic readout, we propose using a photonic readout. This area is anticipated in critical ways using the upconversion method for converting the collected low-energy photons (by advance nanostructures) to high-energy photons of visible light photons (by means of on-chip photonics). The visible light photons can now be detected by our conventional low-cost cameras. In a similar work, mentioned in Table 2, the author used a single-photon sensitive imaging device<sup>145</sup> based on an intracavity design to upconvert MWIR photons to visible photons using a 20-mm long MgO:PPLN (periodically poled lithium niobite) and some bulk optics as shown in Fig. 18. This was done in 2003 when photonics integrated circuit technology was not much developed. Now that our group-IV photonics is reaching new limits for developing on-chip photonic devices (both passive and active), we anticipate the bulk optics part to be transformed to on-chip photonics and hence the development of an all-optical imaging system that will allow for real-time surveillance. This new research has significant potential, specifically considering the modern need for having multispectral and highly sensitive sensors for providing surplus data in real time for the Internet of Things. The technology idea holds a visionary thought to assist the

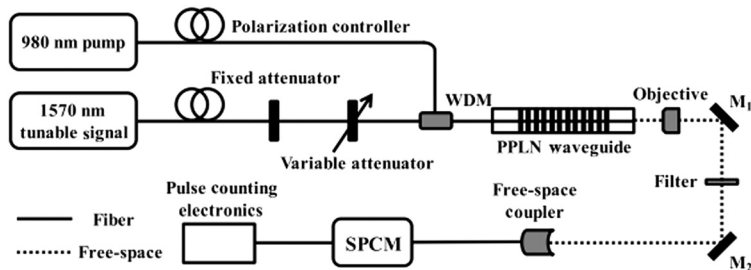


**Fig. 18** Single-photon detector based on frequency upconversion in MgO-doped periodically poled  $\text{LiNbO}_3$ -waveguide: record-low-dark counts and detectable photons.

quantum photonic integration on a chip to disruptively evolve as an alternative to existing uneconomical technologies. Some of the possible areas that would directly benefit from this technology are hyper spectral imaging for remote sensing operations, augmented and virtual reality, autonomous navigation during nighttime for commercial as well as defense sectors. However, like every niche technology, the biggest constraint with this idea is that the overall system becomes a quantum many-body system<sup>167–170</sup> that has a number of complexities involved with moving from mathematical modeling to experimental validations.

#### 4 Conclusion

In conclusion, most recent advancements in the potential areas to be synergized to take a leap toward an all-optical, low-power, light-weight, broad-range IR image sensing system for various applications such as night-vision and bioimaging have been reviewed. First, this paper discussed the most recent developments in IR-absorbers with a focus on longer IR wavelengths. These advancements have been possible due to the advent of new materials having superior electrical and optical properties as well as ease of fabrication with bulk materials such as HgCdTe, InGaAs/GaAs, InSb, and Si/GeSn. The advancements in nanofabrication also enable further engineering the structures of existing QW/QD/QDWELL detectors to perform at higher operating temperatures than their bulk counterparts at low cost. The suitable blend of 2D materials (graphene and BP), with their high sensitivity for low-ambient light conditions and enhanced optical coupling methods (resonant-cavity structures and distributed-grating structures) is making it easy and cost effective to develop state-of-the-art IRPDs as well as IRTDs-based image-sensing FPAs. Finally, photon upconversion enables the possibility of direct image sensing via an all-optical means. With matured upconversion technology, proof-of-concepts for multicolor night-vision devices with a systematic engineering of new materials and advanced nanosurfaces on-chip have been anticipated. With a rapid growth of photonics integrated circuit technology, this paper presented a synergetic approach to developing an all-optical system for capturing real-time images for various image sensing applications in the near future.

#### Acknowledgments

I would like to thank my supervisors Prof. (Dr.) Neena Gupta and Dr. Jyoti Kedia at Punjab Engineering College (deemed to be university), Chandigarh, India, for supporting this research. I would also like to thank Chandigarh University, Punjab, India, for approving my study leave to pursue the doctoral program.

#### References

1. K. Krapels and R. G. Driggers, “Infrared imaging,” *Encycl. Mod. Opt.* **3**, 229–240 (2005).
2. I. J. C. Ottney et al., (12) United States Patent. 2 (2007).
3. R. A. Richwine et al., “Microbolometer sensor model for performance predictions and real-time image generation of infrared scenes and targets,” *Proc. SPIE* **7055**, 70550T (2008).

4. O. Akin and H. V. Demir, "Mid-wave infrared metasurface microlensed focal plane array for optical crosstalk suppression," *Opt. Express* **23**, 27020 (2015).
5. S. Chakrabarti et al., "Indigenous development of  $320 \times 256$  focal-plane array using InAs/InGaAs/ GaAs quantum dots-in-a-well infrared detectors for thermal imaging," *Curr. Sci.* **112**, 1568–1573 (2017).
6. A. Rogalski, "Graphene-based materials in the infrared and terahertz detector families: a tutorial," *Adv. Opt. Photonics* **11**, 314 (2019).
7. C. L. Tan and H. Mohseni, "Emerging technologies for high performance infrared detectors," *Nanophotonics* **7**, 169–197 (2018).
8. A. Rogalski, P. Martyniuk, and M. Kopytko, "Challenges of small-pixel infrared detectors: a review," *Rep. Prog. Phys.* **79**, 46501 (2016).
9. P. Klipstein et al., "Status of cooled and uncooled infrared detectors at SCD, Israel," *Defence Sci. J.* **63**, 555–570 (2013).
10. S. Hafiz et al., "Colloidal quantum dots for thermal infrared sensing and imaging," *Nano Converg.* **6**, 1–22 (2019).
11. K. Minoglou et al., "Infrared image sensor developments supported by the European Space Agency," *Infrared Phys. Technol.* **96**, 351–360 (2019).
12. K. K. Choi et al., "Small pitch resonator-QWIP detectors and arrays," *Infrared Phys. Technol.* **94**, 118–125 (2018).
13. B. Mizaikoff, "Waveguide-enhanced mid-infrared chem/bio sensors," *Chem. Soc. Rev.* **42**(22), 8683–8699 (2013).
14. J. Wang et al., "Resonant-cavity-enhanced mid-infrared photodetector on a silicon platform," *Opt. Express* **18**, 12890–12896 (2010).
15. X. Zhang et al., "Controlling thermal emission by parity-symmetric fano resonance of optical absorbers in metasurfaces," *ACS Photonics* **6**(11), 2671–2676 (2019).
16. E. M. J. Ackson et al., "Two-dimensional plasmonic grating for increased quantum efficiency in midwave infrared *nBn* detectors with thin absorbers," *Opt. Express* **26**, 13850–13864 (2018).
17. A. M. Hoang et al., "High performance bias-selectable three-color short-wave/mid-wave/long-wave infrared photodetectors based on type-II InAs/GaSb/AlSb superlattices," *Sci. Rep.* **6**, 24144 (2016).
18. Q. Durlin et al., "Midwave infrared barrier detector based on Ga-free InAs/InAsSb type-II superlattice grown by molecular beam epitaxy on Si substrate," *Infrared Phys. Technol.* **96**, 39–43 (2019).
19. D. Popa and F. Udrea, "Towards integrated mid-infrared gas sensors," *Sensors* **19**, 2076 (2019).
20. H. Talebi et al., "Fabrication of fast mid-infrared range photodetector based on hybrid graphene–PbSe nanorods," *Appl. Opt.* **54**, 6386 (2015).
21. Q. Zhao et al., "Plasmo-thermomechanical radiation detector with on-chip optical readout," *Opt. Express* **26**, 29638 (2018).
22. P. E. Malinowski et al., "Thin-film quantum dot photodiode for monolithic infrared image sensors," *Sensors (Switzerland)* **17**, 2867 (2017).
23. X. Yu et al., "Narrow bandgap oxide nanoparticles coupled with graphene for high performance mid-infrared photodetection," *Nat. Commun.* **9**, 4299 (2018).
24. A. Rogalski, P. Martyniuk, and M. Kopytko, "InAs/GaSb type-II superlattice infrared detectors: future prospect," *Appl. Phys. Rev.* **4**, 031304 (2017).
25. Y. Zhou et al., "Recent advances in black phosphorus-based photonics, electronics, sensors and energy devices," *Mater. Horizons* **4**, 997–1019 (2017).
26. S. Campione et al., "Realistic full wave modeling of focal plane array pixels," *ACES J.* **32**, 955–959 (2017).
27. B. Jafari and H. Oofi, "High bandwidth and responsivity mid-infrared graphene photodetector based on a modified metal–dielectric–graphene architecture," *Appl. Opt.* **58**, 6280–6287 (2019).
28. K. Hackiewicz, J. Rutkowski, and P. Martyniuk, "Optimal absorber thickness in interband cascade photodetectors," *Infrared Phys. Technol.* **95**, 136–140 (2018).

29. R. Sun et al., "Broadband switching of mid-infrared atmospheric windows by VO<sub>2</sub>-based thermal emitter," *Opt. Express* **27**, 11537 (2019).
30. H. Vora et al., "Bolometric response in graphene based superconducting tunnel junctions," *Appl. Phys. Lett.* **100**, 153507 (2012).
31. J. J. Talghader, A. S. Gawarikar, and R. P. Shea, "Spectral selectivity in infrared thermal detection," *Light Sci. Appl.* **1**, e24 (2012).
32. W. Huang et al., "Current-matching versus non-current-matching in long wavelength interband cascade infrared photodetectors," *J. Appl. Phys.* **122**, 083102 (2017).
33. W. Zhang and J. Yao, "Silicon-based integrated microwave photonics," *IEEE J. Quantum Electron.* **52**, 0600412 (2016).
34. J. Chan et al., "Tools and methodologies for designing energy-efficient photonic networks-on-chip for high-performance chip multiprocessors," in *ISCAS 2010-2010 IEEE Int. Symp. Circuits Syst. Nano-Bio Circuit Fabr. Syst.*, pp. 3605–3608 (2010).
35. G. Carpintero et al., "Photonic integrated circuits for radio-frequency signal generation," *J. Lightwave Technol.* **34**, 508–515 (2016).
36. Q. Fang et al., "WDM multi-channel silicon photonic receiver with 320 Gbps data transmission capability," *Opt. Express* **18**, 5106 (2010).
37. C. Liu et al., "Silicon/2D-material photodetectors: from near-infrared to mid-infrared," *Light: Sci. Appl.* **10**, 123 (2021).
38. L. Zeng et al., "Van der Waals epitaxial growth of mosaic-like 2D platinum ditelluride layers for room-temperature mid-infrared photodetection up to 10.6 μm," *Adv. Mater.* **32**, 2004412 (2020).
39. Y. Ma et al., "Heterogeneously integrated graphene/silicon/halide waveguide photodetectors toward chip-scale zero-bias long-wave infrared spectroscopic sensing," *ACS Nano* **15**, 10084–10094 (2021).
40. S. Pan, N. Boon, and M. Olvera De La Cruz, "Liquid crystal phase transition in epitaxial monolayers of DNA-functionalized nanoparticle superlattices," *ACS Nano* **10**, 9948–9956 (2016).
41. D. Wu et al., "Optically active plasmonic metasurfaces based on the hybridization of in-plane coupling and out-of-plane coupling," *Nanoscale Res. Lett.* **13**, 144 (2018).
42. V. Caligiuri et al., "Resonant gain singularities in 1D and 3D metal/dielectric multilayered nanostructures," *ACS Nano* **11**, 1012–1025 (2017).
43. X. Lan et al., "Programmable supra-assembly of a DNA surface adapter for tunable chiral directional self-assembly of gold nanorods," *Angew. Chem. - Int. Ed.* **56**, 14632–14636 (2017).
44. F. Meder et al., "Ordered surface structuring of spherical colloids with binary nanoparticle superlattices," *Nano Lett.* **18**, 2511–2518 (2018).
45. Q. Shi et al., "Shape transformation of constituent building blocks within self-assembled nanosheets and nano-origami," *ACS Nano* **12**, 1014–1022 (2018).
46. S. K. Maurya et al., "Double negativity in 3D space coiling metamaterials," *Sci. Rep.* **6**, 33683 (2016).
47. C. Yi et al., "Anisotropic self-assembly of hairy inorganic nanoparticles," *Acc. Chem. Res.* **50**, 12–21 (2017).
48. S. Sugumaran et al., "Nanostructured materials with plasmonic nanobiosensors for early cancer detection: a past and future prospect," *Biosens. Bioelectron.* **100**, 361–373 (2018).
49. K. Yang et al., "A terahertz metamaterial biosensor for sensitive detection of microRNAs based on gold-nanoparticles and strand displacement amplification," *Biosens. Bioelectron.* **175**, 112874 (2021).
50. C. M. Soto and W. J. Dressick, "Dual-functionalized virus–gold nanoparticle clusters for biosensing," *Methods Mol. Biol.* **1776**, 533–552 (2018).
51. X. Zheng et al., "Multiscale metallic metamaterials," *Nat. Mater.* **15**, 1100–1106 (2016).
52. L. Chang et al., "Quantum well infrared detector enhanced by local light field (Invited)," *Infrared Laser Eng.* **50**, 20211009 (2021).
53. X. H. Ye et al., "Quantum well micropillar arrays with low filling factor for enhanced infrared absorption," *Hongwai Yu Haomibo Xuebao/J. Infrared Millimeter Waves* **40**, (2021).

54. Z. Chu et al., "Quantum well infrared detectors enhanced by faceted plasmonic cavities," *Infrared Phys. Technol.* **116**, 103746 (2021).
55. P. Guyot-Sionnest, M. M. Ackerman, and X. Tang, "Colloidal quantum dots for infrared detection beyond silicon," *J. Chem. Phys.* **151**, 060901 (2019).
56. S. Jain et al., "I-III-VI core/shell QDs: synthesis, characterizations and applications," *J. Luminesc.* **219**, 116912 (2020).
57. A. Taffelli et al., "Mos<sub>2</sub> based photodetectors: a review," *Sensors* **21**, 2758 (2021).
58. S. Zhang, Y. Hu, and Q. Hao, "Advances of sensitive infrared detectors with HgTe colloidal quantum dots," *Coatings* **10**, 760 (2020).
59. Q. Hao et al., "Development of flexible and curved infrared detectors with HgTe colloidal quantum dots," *Infrared Phys. Technol.* **108**, 103344 (2020).
60. S. K. Al-Ani, "The fabrication of unclassified photodetectors in Iraq," in *Qatar Found. Annu. Res. Conf. Proc.*, Vol. **2016**, pp. EEPPI1181, Hamad bin Khalifa University Press (2019).
61. P. V. K. Yadav et al., "Recent advances in development of nanostructured photodetectors from ultraviolet to infrared region: a review," *Chemosphere* **279**, 130473 (2021).
62. D. D. Sedov, V. K. Kozin, and I. V. Iorsh, "Chiral waveguide optomechanics: first order quantum phase transitions with Z 3 symmetry breaking," *Phys. Rev. Lett.* **125**(26), 263606 (2020).
63. M. Baird et al., "Linear and nonlinear intersubband optical properties of direct band gap GeSn quantum dots," *Nanomaterials* **9**, 124 (2019).
64. M. Baird et al., "Intersubband optical nonlinearity of GeSn quantum dots under vertical electric field," *Micromachines* **10**, 243 (2019).
65. T. Li et al., "Ge-on-Si modulators operating at mid-infrared wavelengths up to 8 μm," *Photonics Res.* **7**, 828 (2019).
66. J. Xavier et al., "Advances in optoplasmonic sensors: combining optical nano/microcavities and photonic crystals with plasmonic nanostructures and nanoparticles," *Nanophotonics* **7**, 1–38 (2018).
67. Z. Yao et al., "Integrated silicon photonic microresonators: emerging technologies," *IEEE J. Sel. Top. Quantum Electron.* **24**, 5900324 (2018).
68. S. Bansal et al., "Bilayer graphene/HgCdTe based very long infrared photodetector with superior external quantum efficiency, responsivity, and detectivity," *RSC Adv.* **8**, 39579–39592 (2018).
69. F. Uzgur and S. Kocaman, "Barrier engineering for HgCdTe unipolar detectors on alternative substrates," *Infrared Phys. Technol.* **97**, 123–128 (2019).
70. M. Kopytko et al., "Photon recycling effect in small pixel p-i-n HgCdTe long wavelength infrared photodiodes," *Infrared Phys. Technol.* **97**, 38–42 (2019).
71. K. M. Yoo et al., "InGaAs membrane waveguide: a promising platform for monolithic integrated mid-infrared optical gas sensor," *ACS Sens.* **5**, 861–869 (2020).
72. Y. Zou et al., "Mid-infrared silicon photonic waveguides and devices [Invited]," *Photonics Res.* **6**, 254–276 (2018).
73. V. W. Brar, M. C. Sherrott, and D. Jariwala, "Emerging photonic architectures in two-dimensional opto-electronics," *Chem. Soc. Rev.* **47**, 6824–6844 (2018).
74. Y. Fang et al., "Mid-infrared photonics using 2D materials: status and challenges," *Lasers Photonics Rev.* **14**, 1900098 (2020).
75. L. Yu et al., "Research progress of uncooled infrared detectors (Invited)," *Hongwai yu Jiguang Gongcheng/Infrared Laser Eng.* **50**, 20211013 (2021).
76. S. Bianconi and H. Mohseni, "Recent advances in infrared imagers: toward thermodynamic and quantum limits of photon sensitivity," *Rep. Prog. Phys.* **83**, 044101 (2020).
77. L. Stabellini et al., "An FDTD approach to the simulation of quantum-well infrared photodetectors," *Opt. Quantum Electron.* **40**, 1085–1090 (2008).
78. K. Prabakaran et al., "Structural, morphological, optical and electrical characterization of InGaN/GaN MQW structures for optoelectronic applications," *Appl. Surf. Sci.* **476**, 993–999 (2019).
79. H. Manis-Levy et al., "Electrical and optical characterization of extended SWIR detectors based on thin films of nano-columnar PbSe," *Infrared Phys. Technol.* **96**, 89–97 (2019).

80. D. Panda et al., “In0.5Ga0.5As bilayer quantum dot heterostructure for mid-infrared photodetection,” *Infrared Phys. Technol.* **94**, 263–266 (2018).
81. D. Das et al., “Vertically coupled hybrid InAs sub-monolayer on InAs Stranski–Krastanov quantum dot heterostructure: toward next generation broadband IR detection,” *IEEE Trans. Nanotechnol.* **19**, 76–83 (2020).
82. D. L. Smith and C. Mailhiot, “Proposal for strained type II superlattice infrared detectors,” *J. Appl. Phys.* **62**, 2545–2548 (1987).
83. D. L. Smith and C. Mailhiot, “Optical properties of strained-layer superlattices with growth axis along [111],” *Phys. Rev. Lett.* **58**, 1264 (1987).
84. R. Müller et al., “High operating temperature InAs/GaSb type-II superlattice detectors on GaAs substrate for the long wavelength infrared,” *Infrared Phys. Technol.* **96**, 141–144 (2019).
85. M. Razeghi et al., “Advances in antimonide-based type-II superlattices for infrared detection and imaging at center for quantum devices,” *Infrared Phys. Technol.* **59**, 41–52 (2013).
86. R. Haydock, V. Heine, and M. J. Kelly, “Electronic structure based on the local atomic environment for tight-binding bands,” *J. Phys. C Solid State Phys.* **5**, 2845 (1972).
87. S. Ferreira, J. Duarte, and S. Frota-Pessa, “Parametrized linear muffin-tin orbitals atomic-sphere approximation tight-binding scheme: the electronic structure of MoRu alloys,” *Phys. Rev. B* **41**, 5627 (1990).
88. A. Rogalski, “Dual-band infrared detectors,” *Hongwai Yu Haomibo Xuebao/J. Infrared Millimeter Waves* **19** (2000).
89. M. B. Reine et al., “Independently accessed back-to-back HgCdTe photodiodes: a new dual-band infrared detector,” *J. Electron. Mater.* **24**, 669–679 (1995).
90. O. O. Cellek, J. L. Reno, and Y. H. Zhang, “Optically addressed near and long-wave infrared multiband photodetectors,” *Appl. Phys. Lett.* **100**, 241103 (2012).
91. Y. Zhang et al., “Suppressing spectral crosstalk in dual-band long-wavelength infrared photodetectors with monolithically integrated air-gapped distributed Bragg reflectors,” *IEEE J. Quantum Electron.* **55**, 4000106 (2019).
92. Y. Zhang, A. Haddadi, and A. Dehzangi, “Suppressing spectral cross-talk in dual-band long-wavelength infrared photodetectors with distributed Bragg reflectors,” *IEEE J. Quantum Electron.* **55**, 1, 1–6 (2018).
93. X. Du et al., “Graphene-based bolometers,” arXiv:1308.4065 (2013).
94. A. Karim and J. Y. Andersson, “Infrared detectors: advances, challenges and new technologies,” *IOP Conf. Ser. Mater. Sci. Eng.* **51**, 012001 (2013).
95. V. Srivastav et al., “Infrared physics & technology exploring novel methods to achieve sensitivity limits for high operating temperature infrared detectors,” *Infrared Phys. Technol.* **61**, 290–298 (2013).
96. P. J. Love et al., “Infrared detectors for ground-based and space-based astronomy applications,” *Proc. SPIE* **4008**, 1254–1267 (2000).
97. X. Guan et al., “Recent progress in short- to long-wave infrared photodetection using 2D materials and heterostructures,” *Adv. Opt. Mater.* **9**, 2001708 (2021).
98. U. Sassi et al., “Graphene-based mid-infrared room-temperature pyroelectric bolometers with ultrahigh temperature coefficient of resistance,” *Nat. Commun.* **8**, 14311 (2017).
99. Q. Guo et al., “Efficient electrical detection of mid-infrared graphene plasmons at room temperature,” *Nat. Mater.* **17**, 986–992 (2018).
100. Q. Guo et al., “Infrared nanophotonics based on graphene plasmonics,” *ACS Photonics* **4**, 2989–2999 (2017).
101. S. Cakmakyapan et al., “Gold-patched graphene nano-stripes for high-responsivity and ultrafast photodetection from the visible to infrared regime,” *Light Sci. Appl.* **7**, 20 (2018).
102. R. Soref, “Emerging SiGeSn integrated-photonics technology,” in *2016 IEEE Photonics Soc. Summer Top. Meet. Ser. SUM 2016*, Vol. 3, pp. 100–101 (2016).
103. H. Tran et al., “High performance Ge0.89Sn0.11 photodiodes for low-cost shortwave infrared imaging,” *J. Appl. Phys.* **124**, 013101 (2018).
104. E. Vitiello et al., “Continuous-wave magneto-optical determination of the carrier lifetime in coherent  $\text{Ge}_{1-x}\text{Sn}_x/\text{Ge}$  heterostructures,” *Phys. Rev. Appl.* **14**, 064068 (2020).

105. D. Imbrenda et al., "Infrared dielectric response, index of refraction, and absorption of germanium-tin alloys with tin contents up to 27% deposited by molecular beam epitaxy," *Appl. Phys. Lett.* **113**, 122104 (2018).
106. P. Pareek, M. K. Das, and S. Kumar, "Numerical analysis of SiGeSn/GeSn interband quantum well infrared photodetector," *Opto-Electron. Rev.* **26**, 149–157 (2018).
107. J. C. Campbell et al., "Photodetectors: UV to IR. Inactive and passive optical components for wdm communications III," *Proc. SPIE* **5246**, 375–388 (2003).
108. K. Strassel et al., "Shortwave infrared-absorbing squaraine dyes for all-organic optical upconversion devices," *Sci. Technol. Adv. Mater.* **22**, 194–204 (2021).
109. A. I. Yakimov et al., "Photovoltaic Ge/SiGe quantum dot mid-infrared photodetector enhanced by surface plasmons," *Opt. Express* **25**(21), 25602–25611 (2017).
110. A. I. Yakimov et al., "Comparison of two-dimensional arrays of gold disks and holes for plasmonic enhancement of Ge/Si quantum dot mid-infrared photodetectors," *Opt. Mater. Express* **8**(11), 3479–3484 (2018).
111. J. P. Perez et al., "New Ga-Free InAs/InAsSb superlattice infrared photodetector," in *6th Int. Conf. Photon. Opt. Laser Technol.*, pp. 232–237 (2018).
112. M. Delmas et al., "Flexibility of Ga-containing Type-II superlattice for long-wavelength infrared detection," *J. Phys. D: App. Phys.* **52**(47), 475102 (2019).
113. D. X. Xu et al., "Photodetectors for 1.3- $\mu\text{m}$  and 1.55- $\mu\text{m}$  wavelengths using SiGe undulating MQWs on SOI substrates," *Int. Soc. Opt. Photon.* **3630**, 50–57 (1999).
114. Z. Zhang et al., "Upconversion nanoprobes: recent advances in sensing applications," *Anal. Chem.* **91**, 548–568 (2019).
115. B. Gu and Q. Zhang, "Recent advances on functionalized upconversion nanoparticles for detection of small molecules and ions in biosystems," *Adv. Sci.* **5**, 1700609 (2018).
116. G. Chen et al., "A series of squaraine dyes: effects of side chain and the number of hydroxyl groups on material properties and photovoltaic performance," *Chem. Mater.* **26**, 1356–1364 (2014).
117. J. Clark and G. Lanzani, "Organic devices for photonics," *Nat. Photonics* **4**(7), 438–446 (2010).
118. C. Duan et al., "Recent progress in upconversion luminescence nanomaterials for biomedical applications," *J. Mater. Chem. B* **6**, 192–209 (2018).
119. G. Jalani et al., "Seeing, targeting and delivering with upconverting nanoparticles," *J. Am. Chem. Soc.* **140**, 10923–10931 (2018).
120. D. J. Garfield et al., "Enrichment of molecular antenna triplets amplifies upconverting nanoparticle emission," *Nat. Photonics* **12**, 402–407 (2018).
121. D. Casanova, "Theoretical modeling of singlet fission," *Chem. Rev.* **118**, 7164–7207 (2018).
122. J. Zhou et al., "Upconversion luminescent materials: advances and applications," *Chem. Rev.* **115**, 395–465 (2015).
123. C. C. Milleville et al., "Engineering efficient photon upconversion in semiconductor heterostructures," *ACS Nano* **13**, 489–497 (2019).
124. L. Liang et al., "Upconversion amplification through dielectric superlensing modulation," *Nat. Commun.* **10**, 1391 (2019).
125. M. Wu et al., "Single-band red upconversion luminescence of Yb<sup>3+</sup>-Er<sup>3+</sup> via nonequivalent substitution in perovskite KMgF<sub>3</sub> nanocrystals," *J. Mater. Chem. C* **4**, 1675–1684 (2016).
126. V. K. Sangwan and M. C. Hersam, "Electronic transport in two-dimensional materials," *Annu. Rev. Phys. Chem.* **69**, 299–325 (2018).
127. S. W. Liu et al., "Transparent organic upconversion devices for near-infrared sensing," *Adv. Mater.* **27**, 1217–1222 (2015).
128. O. P. Dimitriev et al., "Towards white-light generation through upconversion of low-power near-infrared photons," *RSC Adv.* **7**, 16126–16130 (2017).
129. W. Zheng et al., "Near-infrared-triggered photon upconversion tuning in all-inorganic cesium lead halide perovskite quantum dots," *Nat. Commun.* **9**, 3462 (2018).
130. B. Tian et al., "Low irradiance multiphoton imaging with alloyed lanthanide nanocrystals," *Nat. Commun.* **9**, 3082 (2018).
131. S. Artur et al., "Photon avalanche in lanthanide doped nanoparticles for biomedical applications: super-resolution imaging†," *Nanosc. Horizons* **4**, 881–889 (2019).

132. J. Yao and G. Yang, “2D material broadband photodetectors,” *Nanoscale* **12**, 454–476 (2020).
133. C. Ye et al., “Photon upconversion: from two-photon absorption (TPA) to triplet-triplet annihilation (TTA),” *Phys. Chem. Chem. Phys.* **18**, 10818–10835 (2016).
134. H. Ding et al., “Microscale optoelectronic infrared-to-visible upconversion devices and their use as injectable light sources,” *Proc. Natl. Acad. Sci. U. S. A.* **115**, 6632–6637 (2018).
135. X. Qin et al., “Energy-transfer editing in lanthanide-activated upconversion nanocrystals: a toolbox for emerging applications,” *ACS Cent. Sci.* **5**, 29–42 (2019).
136. R. Demur et al., “Near-infrared to visible upconversion imaging using a broadband pump laser,” *Opt. Express* **26**, 13252 (2018).
137. K. Chen et al., “Nanocomposites of carbon nanotubes and photon upconversion nanoparticles for enhanced optical limiting performance,” *J. Mater. Chem. C* **6**, 7311–7316 (2018).
138. S. Junaid et al., “Mid-infrared upconversion based hyperspectral imaging,” *Opt. Express* **26**, 2203 (2018).
139. D. T. U. Fotonik, “Upconversion detection of long-wave infrared radiation from a quantum cascade laser,” *Opt. Mater. Express* **8**, 1313–1321 (2018).
140. K. Du et al., “Wavelength-tunable mid-infrared thermal emitters with a non-volatile phase changing material,” *Nanoscale* **10**, 4415–4420 (2018).
141. X. Zhang et al., “Glasses for seeing beyond visible,” *Chem. A Eur. J.* **14**, 432–442 (2008).
142. S. J. He et al., “Integrated tandem device with photoactive layer for near-infrared to visible upconversion imaging,” *Appl. Phys. Lett.* **112**, 243301 (2018).
143. M. Wu et al., “Solid-state infrared-to-visible upconversion sensitized by colloidal nanocrystals,” *Nat. Photonics* **10**, 31–34 (2016).
144. A. Abulikemu et al., “Solid-state, near-infrared to visible photon upconversion via triplet-triplet annihilation of a binary system fabricated by solution casting,” *ACS Appl. Mater. Interfaces* **11**, 20812–20819 (2019).
145. X. Yu et al., “Atomically thin noble metal dichalcogenide: a broadband mid-infrared semiconductor,” *Nat. Commun.* **9**, 1545 (2018).
146. R. L. Pedersen et al., “Characterization of the NEP of mid-infrared upconversion detectors,” *IEEE Photonics Technol. Lett.* **31**, 681–684 (2019).
147. R. Demur et al., “High sensitivity narrowband wavelength mid-infrared detection at room temperature,” *Opt. Lett.* **42**, 2006 (2017).
148. M. Hermes et al., “Mid-IR hyperspectral imaging for label-free histopathology and cytology,” *J. Opt.* **20**(2), 023002 (2019).
149. M. Mrejen and H. Suchowski, “Multicolor upconversion imaging by Adiabatic SumFrequency Conversion,” *Laser Photon. Rev.* **14**(10) (2019).
150. Y.-P. Seng et al., “Upconversion raster scanning microscope for long-wavelength infrared imaging of breast cancer microcalcifications,” *Biomed. Opt. Express* **9**, 4979–4987 (2018).
151. Y. Tseng, C. Pedersen, and P. Tidemand-Lichtenberg, “Upconversion detection of long-wave infrared radiation from a quantum cascade laser,” *Opt. Mater. Express* **8**, 1313–1321 (2018).
152. T.-H. Wong et al., “Sensitive infrared signal detection by upconversion technique,” *Opt. Eng.* **53**, 107102 (2014).
153. R. L. Pedersen and Z. Li, “Infrared degenerate four-wave mixing with upconversion detection for quantitative gas sensing,” *J. Visualized Exp.* **22**(145), e59040 (2019).
154. A. Barh, C. Pedersen, and P. Tidemand-Lichtenberg, “Ultra-broadband mid-wave-IR upconversion detection,” *Opt. Lett.* **42**, 1504 (2017).
155. K. Wang et al., “Urea-doped carbon dots as fluorescent switches for the selective detection of iodide ions and their mechanistic study,” *RSC Adv.* **11**, 27645–27652 (2021).
156. Q. Xue and G. Xie, “Thermally activated delayed fluorescence beyond through-bond charge transfer for high-performance OLEDs,” *Adv. Opt. Mater.* **9**, 2002204 (2021).
157. Y. V. Vladimirova and V. N. Zadkov, “Quantum optics in nanostructures,” *Nanomaterials* **11**, 1919 (2021).
158. H. Sun et al., “Theoretical insights on the luminescent mechanism of an efficient aggregation-induced nondoped delayed fluorescence emitter using QM/MM method,” *Int. J. Quantum Chem.* **121**, e26490 (2021).

159. J. Liu et al., "Modulated luminescence of lanthanide materials by local surface plasmon resonance effect," *Nanomaterials* **11**, 1037 (2021).
160. M. Rivera, L. Stojanović, and R. Crespo-Otero, "Role of conical intersections on the efficiency of fluorescent organic molecular crystals," *J. Phys. Chem. A* **125**, 1012–1024 (2021).
161. J. Wang and H. Zhang, "Theoretical study on the structural-photophysical relationships of tetra-pt phosphorescent emitters," *Gaodeng Xuexiao Huaxue Xuebao/Chem. J. Chin. Univ.* **42**, 2245–2253 (2021).
162. Z. Shuai, "Thermal vibration correlation function formalism for molecular excited state decay rates," *Chin. J. Chem.* **38**, 1223–1232 (2020).
163. X. Yan et al., "Effects of intramolecular hydrogen bonds on phosphorescence emission: a theoretical perspective," *Appl. Organomet. Chem.* **34**, e5527 (2020).
164. X. Zhou and B. J. Powell, "Quantitative calculations of the non-radiative rate of phosphorescent Ir(III) complexes," *Phys. Chem. Chem. Phys.* **22**, 27348–27356 (2020).
165. S. Lee and W. S. Han, "Cyclometalated Ir(III) complexes towards blue-emissive dopant for organic light-emitting diodes: fundamentals of photophysics and designing strategies," *Inorg. Chem. Front.* **7**, 2396–2422 (2020).
166. B. Fang et al., "Designing organic room temperature phosphorescence with ultralong lifetime by substituent modification," *J. Mater. Chem. C* **9**, 11172–11179 (2021).
167. T. Yoshida, K. Kudo, and Y. Hatsugai, "Non-Hermitian fractional quantum Hall states," *Sci. Rep.* **9**, 16895 (2019).
168. A. Tanaka, A. Tomiya, and K. Hashimoto, "Quantum Manybody Systems, Tensor Networks and Neural Networks," in *Deep Learn. Phys.*, pp. 165–171, Springer, Singapore (2021).
169. J. Zhao et al., "Higher-form symmetry breaking at Ising transitions," *Phys. Rev. Res.* **3**, 033024 (2021).
170. T. Langen, R. Geiger, and J. Schmiedmayer, "Ultracold atoms out of equilibrium," *Annu. Rev. Condens. Matter Phys.* **6**, 201 (2015).
171. A. Boucherif et al., "InAsSb based mid-infrared optical upconversion devices operable at thermoelectric temperatures," *Electron. Lett.* **44**(4), 312–313 (2008).
172. Y. Ma et al., "Mammalian near-infrared image vision through injectable and self-powered retinal nanoantennae," *Cell* **177**(2), 243–255 (2019).

**Neena Gupta** received her BE degree in electronics and communication engineering (ECE) in 1988, her ME degree in electronics in 1992, and her PhD in optical communication in 2002 from Punjab University. She is a professor in the ECE Department, Punjab Engineering College (deemed to be University), Chandigarh, India. She is a senior member of IEEE, having vast teaching and research experience. Her research interests focus on optical communication. She has contributed to various journals and conferences.

**Jyoti Kedia** received her master's degree in 2004 and her PhD in optical communication in 2017 from Thapar University, Patiala, India. She is an assistant professor in the ECE Department, Punjab Engineering College (deemed to be University), Chandigarh, India. Her research interests include optical sensors, passive optical networks, integrated optics, photonics, optical sensors, and VLSI. She has published more than 40 research/technical papers in various international/national journals and conferences.

**Anurag Sharma** received his BE degree in ECE from Himachal Pradesh University, Shimla, India, in 2013, his master's degree from Chandigarh University, Punjab, India, in 2016, and is pursuing his PhD at Punjab Engineering College (deemed to be University), Chandigarh, India. He has been an assistant professor in the Department of Mechatronics Engineering, Chandigarh University, Punjab, India, since 2016. His areas of research include nanophotonic sensing, integrated layout design, and AI-enabled computational device modeling. He has contributed to a few scientific journals.